Main text

The genetic architecture of the load linked to dominant and recessive self-incompatibility alleles in *Arabidopsis halleri* and *A. lyrata*

Le Veve Audrey[1,2], Genete Mathieu[1], Lepers-Blassiau Christelle[1], Ponitzki Chloé[1], Poux Céline[1], Vekemans Xavier[1], Durand Eleonore[1], Castric Vincent[1*]

[1]*Univ. Lille, CNRS, UMR 8198 – Evo-Eco-Paleo, F-59000 Lille, France*

[2]*Current address: Department of Botany, Faculty of Science, Charles University, Benátská 2, CZ-128 01 Prague, Czechia*

* *Correspondence : vincent.castric@univ-lille.fr*

Abstract

The long-term balancing selection acting on mating-types or sex determining genes is expected to lead to the accumulation of deleterious mutations in the tightly linked chromosomal segments that are locally "sheltered" from purifying selection. However, the factors determining the extent of this accumulation are poorly understood. Here, we took advantage of variations in the intensity of balancing selection along a dominance hierarchy formed by alleles at the sporophytic self-incompatibility system of the Brassicaceae to compare the pace at which linked deleterious mutations accumulate among them. We first experimentally measured the phenotypic manifestation of the linked load at three different levels of the dominance hierarchy. We then sequenced and phased polymorphisms in the chromosomal regions linked to 126 distinct copies of *S*-alleles in two populations of *Arabidopsis halleri* and three populations of *A. lyrata*. We find that linkage to the *S*-locus locally distorts phylogenies over about 10-30kb along the chromosome. The more intense balancing selection on dominant *S*-alleles results in greater fixation of linked deleterious mutations, while recessive *S*-alleles accumulate more linked deleterious mutations that are segregating. Hence, the structure rather than the overall magnitude of the linked genetic load differs between dominant and recessive *S*-alleles. Our results have consequences for the long-term evolution of new *S*-alleles, the evolution of dominance modifiers between them, and raise the question of why the non-recombining regions of some sex and mating type chromosomes expand over evolutionary times while others, such as that the *S*-locus of the Brassicaceae, remain restricted to small chromosomal regions.

Keywords: Supergene, sheltered load, mating types, balancing selection, genetic dominance, S-locus.

Introduction

The existence of sexes or mating-types leads to one the strongest forms of long-term balancing selection, and is often associated with clusters of polymorphisms around sex/mating-type controlling regions kept together by structural rearrangements. In some cases, such rearrangements can span almost entire chromosomes, *e.g.* sex chromosomes in mammals (Katsura et al., 2012) or mating-type chromosomes in ascomycete fungi (Hartmann et al., 2021), while in others they remain limited to relatively small genomic regions, e.g. chromosomal inversions controlling male reproductive morphs in the ruff (Lamichhaney et al., 2016), mating-type loci in some basidiomycete fungi, segregating indels controlling pin *vs*. thrum floral morphs in Primula (Cocker et al., 2018). The long-term balancing selection acting on these systems is expected to lead to the accumulation of deleterious mutations in the tightly linked chromosomal segments that are "sheltered" from purifying selection by the presence of the balanced polymorphism (Uyenoyama, 1997; Uyenoyama, 2005). These deleterious mutations can have drastic short- and long-term consequences for the evolution of the species, and determining the processes by which they accumulate is crucial to understand how the rearranged regions can either expand along the chromosomes or conversely remain restricted to limited genomic tracts (Jay et al,. 2021; Jay et al,. 2022).

Self-incompatibility (SI) is a genetic mechanism allowing recognition and rejection of self-pollen by hermaphrodite individuals, thereby preventing inbreeding and promoting outcrossing in hermaphroditic plant species (Nettancourt, 2001). In the Brassicaceae family, SI is controlled by a single non-recombining chromosomal region, the *S*-locus (Schopfer et al., 1999; Kusaba et al., 2001). SI is one of the most prominent examples of long-term balancing selection (Uyenoyama, 2003), and as such deleterious mutations are expected to accumulate in very close genetic linkage to the *S*-alleles because of the indirect effects of linked selection (Uyenoyama, 2005). Population genetics models predict that recessive deleterious variants should accumulate within specific *S*-allele lineages (Uyenoyama, 2003; Llaurens et al., 2009a), and should then be reshuffled among them by recombination. However, due to the technical difficulty of phasing polymorphisms, this process has rarely been characterised in detail (Castric and Vekemans, 2004).

A key feature of sporophytic SI systems, also shared by sex chromosomes, is the existence of dominance interactions between *S*-alleles. While most individuals are heterozygous at the *S*-locus and thus carry two different *S*-alleles, only one of them is generally expressed at the phenotypic level. This is especially true for the pollen specificity, where *S*-alleles follow a complex genetic dominance hierarchy (Llaurens et al., 2008; Durand et al., 2014). In *Arabidopsis lyrata* and *A. halleri*, the S-alleles are distributed into four classes of dominance, with increasing dominance from class I to class IV and linear dominance also observed inside some of the classes. Similar patterns of dominance between S-alleles occur in Brassica species, but with only two classes (Hatakeyama et al., 1998; Kakizaki et al., 2003; Yasuda et al., 2017). This system is genetically determined and controlled by small RNAs molecules produced by dominant *S*-alleles that are able to target and repress expression of the recessive *S*-alleles in pollen (Durand et al., 2014; Yasuda et al., 2017). The evolutionary properties of *S*-alleles are expected to vary in a predictable manner along the dominance hierarchy because balancing selection acts more strongly on dominant than on recessive *S*-alleles, as the latter are often masked at the phenotypic level (Billiard et al., 2007). As a result, the dynamics of accumulation of deleterious variation may differ in close linkage with dominant *vs* recessive *S*-alleles. Specifically,

recessive *S*-alleles can form homozygous combinations in natural populations more often than dominant *S*-alleles (Billiard et al., 2007), such that recombination can occur occasionally between distinct gene copies of the same recessive *S*-allele, providing the opportunity for the linked recessive deleterious mutations to be purged from within the *S*-locus itself. In addition, because recessive *S*-alleles reach higher population frequencies (Billiard et al., 2006; Llaurens et al., 2008), purifying selection on linked deleterious variants is expected to have higher efficacy among gene copies of recessive than dominant *S*-alleles. This is expected to result in a higher fixation probability of deleterious variants linked to the class of dominant *S*-alleles than to the class of recessive *S*-alleles (Llaurens et al., 2009a). Thus, the level of dominance of S-alleles determines the intensity of purifying selection acting upon them. This situation closely resembles that of the differential evolution of sex chromosomes, where Y chromosomes (similar to dominant S-alleles) tend to accumulate more deleterious variation than X chromosomes (similar to recessive S-alleles, Llaurens et al. 2009a; Goubet et al. 2012). Empirical support for this simple prediction has been conflicting, though. Based on phenotypic measurements in *A. halleri,* Llaurens et al. (2009a) observed a decrease of fitness associated by enforced homozygosity for one of the most dominant *S*-alleles (Ah15) but not for the most recessive *S*-allele of the allelic series (Ah01). In contrast, Stift et al. (2013) observed no effect of dominance on the genetic load linked to three dominant *vs*. recessive *S*-alleles in a natural population of the closely related *A. lyrata*. Hence, the data available so far are inconclusive, but are restricted to very small numbers of *S*-alleles. They are also based on inherently limited phenotypic measurements, seriously limiting the power of the comparisons, and preventing proper generalisation of the effect of the intensity of balancing selection on the accumulation of linked deleterious variation.

In this study, we combined phenotypic, genomic and theoretical approaches to finely dissect the patterns of accumulation of deleterious variation linked to the *S*-locus supergene in *A. halleri* and *A. lyrata*, depending on dominance levels of S-allele. We first extended the phenotypic approach of Llaurens et al. (2009a) to a series of additional *S*-alleles from the same local *A. halleri* population to evaluate the effect of *S*-allele dominance on the sheltered load. We then used parent-offspring trios and targeted genome re-sequencing to directly quantify the accumulation of putative deleterious mutations linked to phased dominant *vs*. recessive *S*-alleles in two *A. halleri* and three *A. lyrata* natural populations. Finally, we used stochastic simulations to refine the theoretical predictions about the patterns of accumulation of recessive deleterious mutations linked to dominant *vs.* recessive *S*-alleles. Overall, our results provide a more nuanced view of the effect of the intensity of balancing selection on the sheltered load, in which the structure of the sheltered load rather than its magnitude differs among *S*-alleles from different dominance classes.

Results

The genetic load linked to the S-locus varies among S-alleles, but is not correlated with dominance.

We first expanded the experimental approach of Llaurens et al. (2009a) to phenotypically evaluate the effect of *S*-allele dominance on the intensity of the sheltered load. The previous study focused on three *S*-alleles (Ah01, Ah02 and Ah15; Llaurens et al., 2009a). Here we included two *S*-alleles from the same local population (Nivelle, France): Ah03 and Ah04, and included Ah01 again for comparative purposes. In the Arabidopsis genus, *S*-alleles have been shown to form a complex dominance hierarchy (Llaurens et al., 2008; Durand et al., 2014). This hierarchy is largely associated with the phylogeny of *S*-alleles (Durand et al., 2014), and at least four phylogenetic classes (I, II, III and IV) have been

116 described, from the most recessive (class I) to the most dominant of *S*-alleles (class IV). Dominance
117 interactions also exist among *S*-alleles within classes, such that these five *S*-alleles form the following
118 dominance hierarchy (Llaurens et al., 2008; Durand et al., 2014): Ah01<Ah03<Ah02<Ah04<Ah15, from
119 the most recessive (Ah01) to the most dominant (Ah15). To reveal the linked load, we enforced
120 homozygosity at the *S*-locus using controlled crosses between parental individuals sharing a given *S*-
121 allele that was masked by different dominant *S*-alleles (*e.g.*, to obtain Ah_xAh_x homozygotes we
122 deposited pollen from a Ah_xAh_y plant, where $Ah_y>Ah_x$, on pistils of a Ah_xAh_z plant where z≠y, or on a
123 Ah_xAh_x pistil when available; table S1). We obtained 399 offspring from a total of six such crosses. Note
124 that our experimental procedure differs slightly from that of Llaurens et al. (2009a) in that their
125 procedure required a CO_2 treatment to bypass the SI system and obtain selfed offspring, while here
126 we took advantage of the dominance interactions to obtain outcrossed *S*-locus homozygous
127 individuals that we phenotypically compared to their full-sibs with *S*-locus heterozygous genotypes.
128 Note also that the *S*-locus homozygous offspring we obtained contain distinct gene copies of a given
129 *S*-allele lineage. Hence, they could in principle carry distinct suites of linked deleterious mutations in
130 case these mutations segregate within *S*-allele lineages.

131 We first tested whether homozygosity at the *S*-locus affected survival by measuring for each cross the
132 proportion of homozygotes at the *S*-locus reaching the reproductive stage for three *S*-alleles (in two
133 replicate families per *S*-allele, Table S1). The proportion of Ah01/Ah01 and Ah04/Ah04 homozygotes
134 surviving to the reproductive stage was consistent with mendelian expectations in their respective
135 families. However, we observed a significant decrease of Ah03/Ah03 homozygotes at the reproductive
136 stage compared with Mendelian expectations (Table 1), whereas the observed proportion of the Ah03
137 *S*-allele among heterozygous individuals did not depart from expectations (2/3=0.67; Table 1). Thus,
138 the increased mortality is associated with Ah03 homozygosity, rather than with a lower performance
139 of individuals carrying the Ah03 *S*-allele itself. Overall, a genetic load was thus observed linked to the
140 Ah03 *S*-alleles, which is at an intermediate level of dominance, but neither to the most dominant
141 (Ah04) nor to the most recessive (Ah01) *S*-allele. Hence, these observations do not support a positive
142 correlation between *S*-allele dominance and the magnitude of the sheltered load.

143 ***Table 1: Proportion of S-locus homozygous offspring having reached the reproductive stage for three***
144 ***different S-alleles.*** *The test is performed relative to the expected proportion of homozygous genotypes*
145 *in the offspring (25% when both parents are heterozygous; 50% when one of the parents is*
146 *homozygous and the other heterozygous).*

***S*-allele**	**Level of dominance**	**Number of seedlings having reached the reproductive stage**	**Observed proportion of homozygotes**	**Ratio of the observed to expected proportion of homozygous genotypes (*p*-value[a])**	**Number of heterozygotes with the *S*-allele (*p*-values[a])**
Ah01	I	35	0.29	1.14 (0.76)	19 (0.40; 0.90)
Ah03	II	27	**0.074**	**0.3 (0.02)**	17 (1; 0.69)
Ah04	III	96	0.479	0.96 (0.39)	50

147 [a] *p-values were obtained after 10,000 random permutations, respectively. Values departing from*
148 *Mendelian expectations are figured in bold. For Ah04, the maternal parent was Ah04/Ah04, so all*
149 *heterozygous offspring carried the S-allele.*

150 Next we measured thirteen vegetative and reproductive traits in the resulting families and compared
151 offspring that were homozygous for their *S*-alleles with their full sibs that were heterozygous (Fig. 1).
152 We first used permutations to test whether the mean trait value of homozygotes differed from that
153 in heterozygotes. Overall, with a single exception, we found no effect of homozygosity at the *S*-locus
154 on variation of the traits measured (Fig. 1; Table S2). The maximum length of flowering stems was the
155 exception to this general pattern, with longer reproductive stems for *S*-locus homozygous than
156 heterozygous genotypes, hence in the opposite direction from our expectation of lower fitness in
157 homozygotes. For this trait, there was significant variation among replicate families for homozygotes
158 of the recessive allele Ah01 but not of the dominant allele Ah04 (Table S3). We then used generalised
159 linear models (GLM) to evaluate the effect of dominance (considered as a continuous variable with
160 fixed effect) on the mean phenotypic value of homozygotes compared to heterozygotes for each trait
161 (Table S4; treating family of origin, attacks by phytopathogens, phytophagous and oxidative stress as
162 random effects whenever necessary). We also observed no effect of *S*-allele dominance on the
163 contrast between *S*-locus homozygotes and heterozygotes for any of these traits. A single of the
164 thirteen traits was an exception to this general pattern, but again the effect was in the opposite
165 direction from our expectation, with an earlier rather than delayed appearance of the first leaf for
166 homozygotes of more dominant *S*-alleles; Table S4). Overall, our phenotypic results confirmed the
167 presence of a detectable linked load on some phenotypic traits (survival; time to produce the first
168 leaf), but we could not replicate the observation of Llaurens et al. (2009a) that dominant *S*-alleles carry
169 a more severe deleterious load than recessive *S*-alleles, even though our samples were obtained from
170 the same local population.

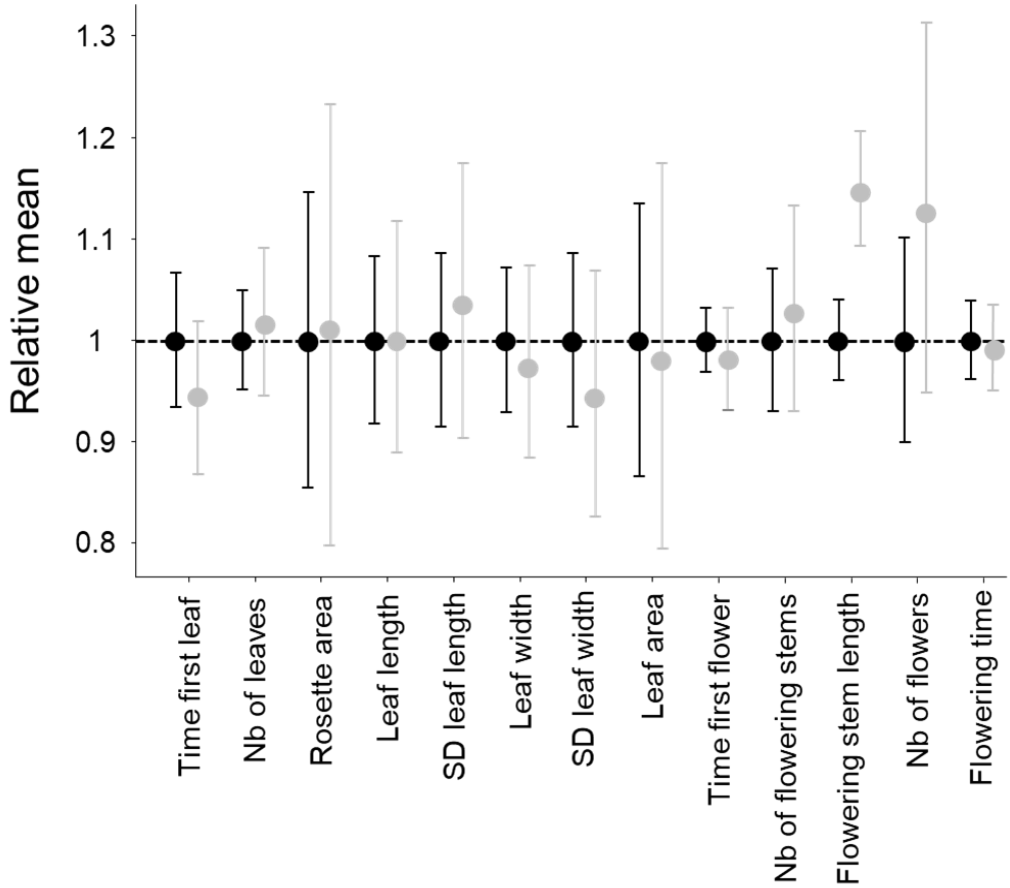

Figure 1: Effect of homozygosity at the S-locus on 13 phenotypic traits compared to heterozygotes. *For each trait, the phenotypic values in homozygotes (in grey) were normalised relative to the mean phenotypic values in heterozygotes (in black). The distributions were obtained by 10,000 random permutations. SD: Standard Deviation.*

S-alleles are associated with specific sets of tightly linked mutations.

The model of the sheltered load assumes that distinct *S*-allele lineages carry specific sets of linked deleterious mutations, but to our knowledge this prediction was never tested directly. We combined a parent-offspring trio approach with sequencing of the *S*-locus flanking regions to phase the mutations segregating in the *S*-locus flanking regions with their respective *S*-alleles. Briefly, we used a previously developed sequence capture protocol specifically targeting the nucleotide sequences over 75 kb on each side of the *S*-locus along with a series of 100 control regions from throughout the genome (Le Veve et al., 2023), and we analysed nucleotide sequence polymorphism (including only invariant and biallelic SNPs), based on the *A. lyrata* reference genome (Hu et al., 2011). We define a haplotype as a unique combination of mutations along the phased chromosome, and a *S*-allele lineage as the collection of gene copies of a given functional *S*-allele (different functional *S*-alleles are distinguished based on their strong sequence divergence at the *S*-locus pollen and pistil genes). Different gene copies within an *S*-allele lineage can thus be associated with distinct linked haplotypes in the flanking regions. The *S*-alleles were identified based on short reads sequences according to a previously published method (Genete et al., 2020). We analysed two closely related *A. halleri* populations from Europe (Nivelle and Mortagne) and three allogamous *A. lyrata* populations from North America (IND, PIN and TSS; Foxe et al., 2010). Overall, we were able to reconstruct 34 haplotypes

193 linked to a total of 12 distinct *S*-allele lineages in Nivelle, 38 haplotypes linked to 11 distinct *S*-allele
194 lineages in Mortagne and 16, 22 and 16 haplotypes associated with 6, 7 and 5 distinct *S*-allele lineages
195 in populations IND, PIN and TSS, respectively (Table S5). Nine of the *S*-alleles were shared between
196 the two *A. halleri* populations (Ah01, Ah03, Ah04, Ah05, Ah12, Ah20, Ah24, Ah25 and Ah59). In the
197 populations of *A. lyrata*, four *S*-alleles were shared between PIN and TSS (Ah01*, Ah03*, Ah18* and
198 Ah63*), five *S*-alleles were shared between PIN and IND (Ah01*, Ah03*, Ah46* and Ah63*), four *S*-
199 alleles were shared between IND and TSS (Ah01*, Ah03*, Ah31* and Ah63*), and three were shared
200 across all three (Ah01*, Ah03* and Ah63*). Note that for convenience, we used *A. halleri* notations
201 (with the addition of a *) to refer to the trans-specifically shared *A. lyrata S*-alleles. Altogether, we
202 were able to obtain the phased flanking sequences of 126 *S*-locus haplotypes, comprising a total of
203 4,854 variable sites. This provides considerable power to evaluate the local accumulation of linked
204 mutations across *S*-alleles of different levels of dominance and to examine their patterns of
205 conservation between populations and between species.

206 Mutations in the *S*-locus flanking regions can be exchanged between *S*-alleles by recombination, and
207 between local populations by migration (Charlesworth, 2006). The relative time scale of these two
208 processes (recombination *vs.* migration) determines the distribution of the linked mutations. To
209 capture the chromosomal extent of this effect of linkage to *S*-alleles, we developed a new phylogenetic
210 method comparing the likelihood of two contrasted topologies of interest in overlapping windows
211 along the chromosome: (1) the topology clustering haplotypes by the populations where they came
212 from vs. (2) the topology clustering them by the *S*-allele to which they are linked (Fig 2A). This allowed
213 us to evaluate the progressive shift from a predominant topology by *S*-alleles close to the *S*-locus to a
214 topology by populations further along the chromosome and in unlinked control regions (Fig. 2B). The
215 difference in log likelihood between the two topologies decreased significantly with distance to the *S*-
216 locus (Pearson coefficient = -0.015 and -0.010 for *A. halleri* and *A. lyrata* respectively; *p*-values $<2^{e-16}$).
217 In *A. halleri*, the topology grouping haplotypes by populations became more likely than the topology
218 grouping them by *S*-alleles at a distance of around 30kb from the *S*-locus, but even at a distance of
219 50kb the phylogenetic structure was still different from that in regions unlinked to the *S*-locus used as
220 controls for the genomic background (Le Veve et al., 2023; Fig 2B). In *A. lyrata,* the shift was even
221 more rapid (within 10-15kb), although we note that the phylogenetic structure of the control regions
222 was less resolved (Fig 2B). To evaluate these patterns more directly we first examined the data using
223 a Major Component Analysis (MCA, a modified version of PCA adapted to binary data, Fig S1 and S2)
224 and using simple phylogenetic reconstructions (Fig S3, S4, S5 and S6). We confirmed that haplotypes
225 linked to a given *S*-allele tended to cluster together in the most tightly linked region, and that this
226 grouping by *S*-alleles was progressively lost in favour of a grouping by population of origin in the most
227 distant regions. Following Kamau et al. (2007), we compared the fixation index F_{ST} among local
228 populations and among *S*-alleles in *A. lyrata* and *A. halleri*. In both *A. halleri* and *A. lyrata*, F_{ST} values
229 among *S*-alleles were high in regions close to the *S*-locus and quickly decreased to reach the
230 background level (Fig. S7) as the distance from the *S*-locus increased. In parallel, the differentiation
231 among populations followed roughly the opposite pattern, i.e. it was initially low in regions close to
232 the *S*-locus (as expected under strong balancing selection) and increased up to background level within
233 the first few kilobases (Fig. S7). In line with our phylogenetic analysis, differentiation between
234 populations started to exceed differentiation between *S*-alleles much closer to the *S*-locus in the *A.*
235 *lyrata* than in the *A. halleri* populations (Fig S3, S4, S5 and S6). Finally, we explored the fine-scale
236 patterns of association within populations between individual *S*-alleles and SNP in the linked and the

237 control regions (Fig S8). As expected, the vast majority of significant associations were found for the
238 most closely linked SNPs. With a single exception, all *S*-alleles were associated with unique SNPs in the
239 50kb region around the *S*-locus, albeit with substantial heterogeneity among *S*-alleles in the patterns
240 and extent of associations that they show (Fig S8). Overall, our results indicate that due to limited
241 recombination, the *S*-alleles carry a specific set of polymorphic sites in the linked region. This
242 association fades away for more distant sites over a few kilobases, where population structure
243 becomes predominant, as in the rest of the genome. Hence, different *S*-alleles are associated with
244 specific sets of tightly linked mutations, but only within 10-30kb.

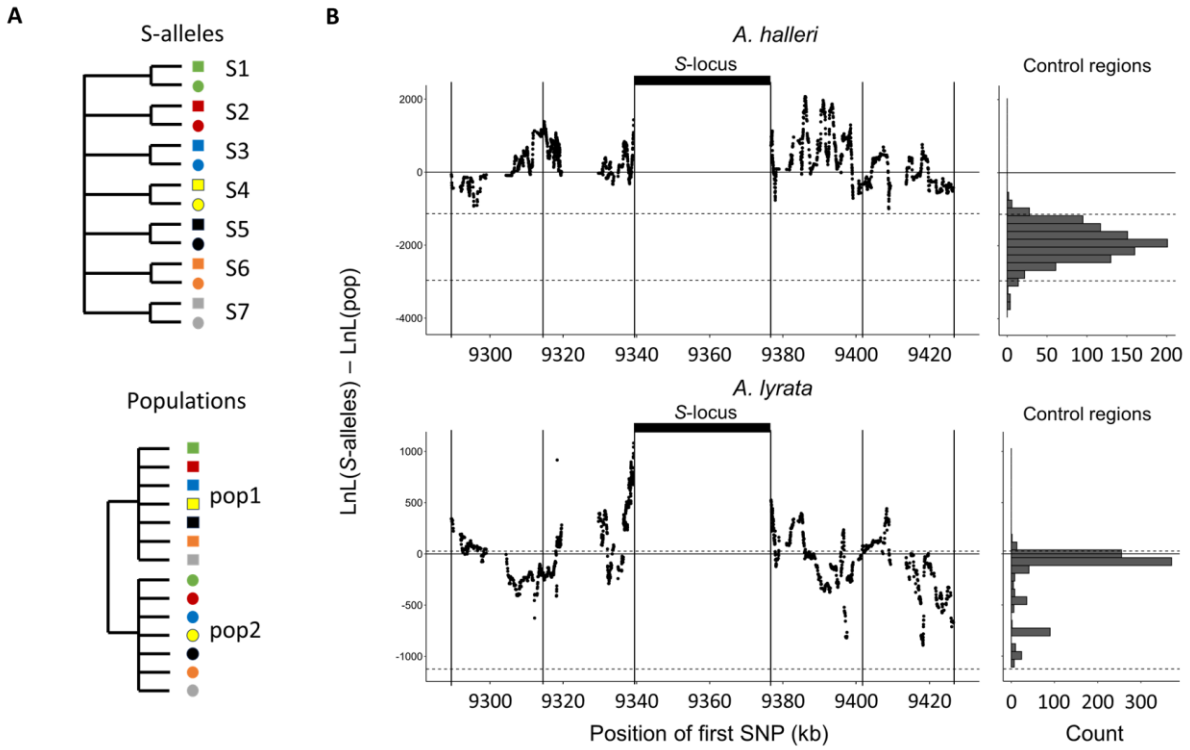

245

246 ***Figure 2: Linkage to the S-locus locally distorts the phylogenetic relationships.*** *A. The two topologies*
247 *of interest cluster haplotypes either by the S-allele to which they are linked (top) or by the populations*
248 *where they came (bottom). Different S-alleles are represented by symbols of different colours, different*
249 *populations of origin are represented by symbols of different shapes. B. Difference in log likelihood of*
250 *the two topologies of interest. Dots correspond to the difference in log likelihood for overlapping series*
251 *of 50 SNPs around the S-locus for A. halleri (top panel) and A. lyrata (bottom panel). Positive values*
252 *correspond to chromosomal positions where the topology by S-alleles explains the phylogeny of*
253 *haplotypes better than the topology by populations. The right panels show the difference in log*
254 *likelihood in the control regions. 2.5 and 97.5 percentiles of the distribution in the control regions are*
255 *indicated by dashed lines.*

256 *No overall evidence that dominant S-alleles accumulate more linked deleterious mutations.*

257 Llaurens et al. (2009a) predicted that recessive deleterious mutations should fix more readily when
258 linked to dominant *S*-alleles than when linked to recessive *S*-alleles. To test this prediction, we
259 investigated the correlation between the level of dominance of the *S*-alleles and their total number of
260 0-fold degenerate mutations (S_{0f}) or the ratio of 0-fold to 4-fold mutations (S_{0f}/S_{4f}) for the phased

261 haplotypes, assuming that the vast majority of 0-fold degenerate mutations are deleterious. Based on
262 the results presented above and the results of our previous study (Le Veve et al., 2023), for the rest of
263 our analyses we focused on the phased haplotypes over the first 25 kb on either side of the *S*-locus.
264 We found no overall effect of dominance on S_{0f} (p-values= 0.54 and 0.07 for *A. halleri* and *A. lyrata*
265 respectively; Fig. 3; Table S6) or S_{0f}/S_{4f} (p-values= 0.54 and 0.07 for *A. halleri* and *A. lyrata* respectively;
266 Table S6). Extending the analysis to all non-synonymous mutations, or to deleterious mutations
267 predicted by SIFT4G and by SNPeff led to identical conclusions (Table S6). Overall, our genomic results
268 did not confirm the prediction that dominant *S*-alleles accumulate a larger number of putatively
269 deleterious mutations in their linked regions. We note that the particular *S*-allele whose sheltered load
270 was quantified in Llaurens et al. (2009a) (Ah15, red arrow on Fig 3A) appears to be one of the *S*-alleles
271 associated with the highest number of 0-fold degenerate mutations among all *S*-alleles of the most
272 dominant class (class IV).

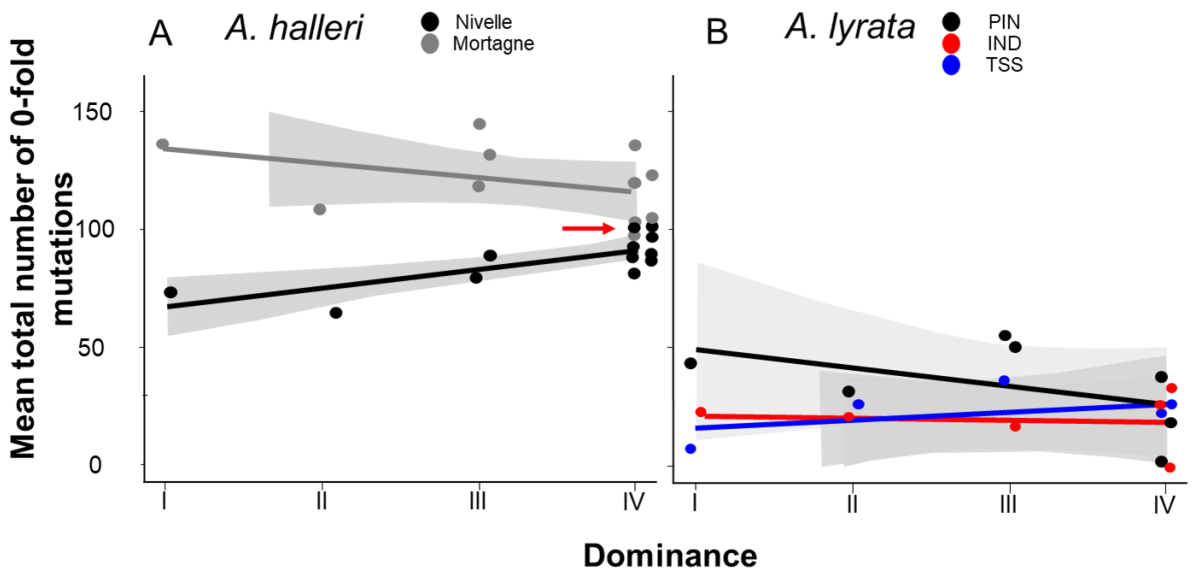

273

274 ***Figure 3: No overall effect of S-allele dominance on the total number of 0-fold degenerate mutations***
275 ***(S_{0f}) in the linked genomic regions within 25kb.*** *Each dot represents the mean number of mutations*
276 *observed among haplotypes linked to one S-allele in one population. The correlations evaluated by a*
277 *GLM are represented by lines, with confidence intervals represented in grey. The dominance was*
278 *considered as a continuous variable. A: A. halleri. Black dots correspond to the Nivelle population, grey*
279 *dots to the Mortagne population. The red arrow points to the copy of Ah15, corresponding to the S-*
280 *allele whose sheltered load was phenotypically characterised by Llaurens et al. (2009a) in Nivelle. B: A.*
281 *lyrata. Red dots correspond to the IND population, black dots to the PIN population and blue dots to*
282 *the TSS population.*

283 *The structure of the linked genetic load differs between dominant and recessive S-alleles.*

284 Theory predicts that dominant *S*-alleles should fix linked recessive deleterious mutations with a higher
285 probability than recessive *S*-alleles (Llaurens et al., 2009a), but in natural populations we observed no
286 difference in the total number of putatively deleterious linked to dominant *vs*. recessive *S*-alleles. To
287 clarify this discrepancy, we took advantage of our sequencing of multiple copies of *S*-alleles to consider
288 separately the fixed and the segregating mutations linked to each of the *S*-allele lineages. For each

population, we included only mutations that were segregating, and excluded those that were locally fixed. In agreement with the prediction of Llaurens et al. (2009a), we observed that lineages of dominant *S*-alleles do indeed tend to fix deleterious mutations more readily (Fig. 4; Table S6). This conclusion held true when extending the analysis to all non-synonymous mutations and to the lowly and the moderately deleterious mutations predicted by SNPeff (Table S6). This was also true using SIFT4G to identify deleterious mutations, with the only exception of a non-significant correlation for *A. halleri,* which might be due to the low number of nucleotide sites included in the SIFT4G database, resulting in low power to detect differences (Table S6). The fact that dominant *S*-alleles tend to fix deleterious mutations more readily but do not accumulate a larger total number of deleterious mutations is explained by the fact that the structure of the genetic load differs between dominant and recessive *S*-alleles: the dominant *S*-alleles tend to have more fixed deleterious mutations, but the recessive *S*-alleles compensate by accumulating a larger number of segregating mutations, resulting in similar numbers of deleterious mutations overall in most of the populations.

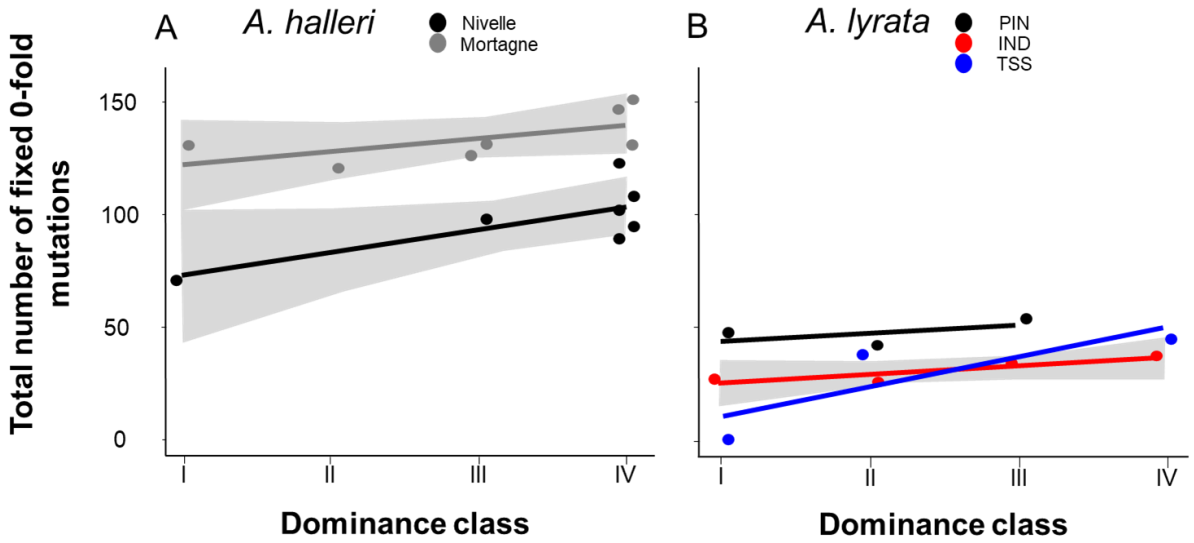

Figure 4: The number of 0-fold degenerate mutations fixed in the 25kb regions flanking the S-locus increases with dominance of the S-allele associated. *Each dot represents the value obtained for haplotypes linked to one S-allele in one population. The correlations evaluated by a GLM are represented by lines, with confidence intervals represented in grey. The dominance was considered as a continuous variable. A: A. halleri. Black dots correspond to the Nivelle population, grey dots to the Mortagne population. B: A. lyrata. Red dots correspond to the IND population, black dots to the PIN population, blue dots to the TSS population.*

Motivated by these empirical observations, we built upon the model by Llaurens et al. (2009a), who showed that linked deleterious mutations (especially fully recessive ones) are expected to fix within dominant S-allele lineages more readily than within recessive S-allele lineages. Here, we adapted the model to focus not only on fixed deleterious mutations, but also on those that are segregating within allelic lineages. Our stochastic simulations confirmed that, at equilibrium, dominant *S*-alleles tend to accumulate a larger number of recessive deleterious mutations that are fixed among gene copies within *S*-allele lineages (Fig. 5A). In contrast, the number of segregating linked mutations was higher for recessive than for dominant *S*-alleles (Fig. 5B). These two effects eventually compensate each

other, such that in the end the mean number of linked deleterious mutations per copy of S-allele was not expected to change between dominant and recessive *S*-alleles (Fig. 5C). These predictions are in line with our genomic observations and suggest that the dominance level of *S*-alleles modifies the structure of the genetic load they shelter: dominant *S*-alleles accumulate more fixed deleterious mutations, but recessive *S*-alleles accumulate more segregating mutations, resulting in an equivalent load overall.

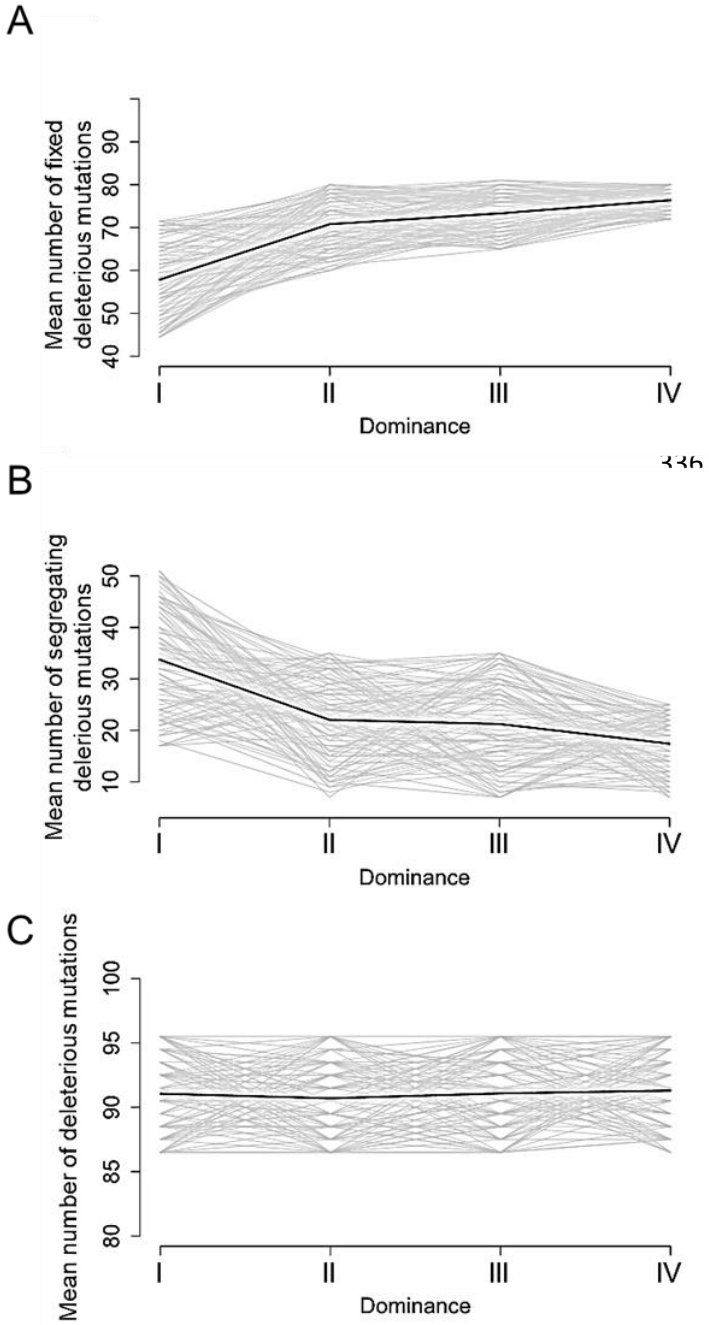

Figure 5: Stochastic simulations confirm the contrasted architecture of the load of deleterious mutations linked to dominant vs. recessive S-alleles. *Number of fixed (A), segregating (B) and the mean number of deleterious mutations (C) linked to S-alleles at four different levels of dominance (I<II<III<IV). The means (bold lines) were estimated per S-allele dominance classes over 100 replicate simulations after discarding an initial burn-in of 100,000 generations. h=0. s=0.01.*

Discussion

The genetic load linked to the S-locus is detectable and is manifested on different phenotypes

352 Our results contribute to a growing body of evidence confirming that the accumulation of deleterious
353 mutations linked to strongly balanced allelic lines can be substantial, and that their effect can be
354 detected at the phenotypic level (Lane and Lawrence, 1995; Stone, 2004; Llaurens et al., 2009a; Mena-
355 Ali et al., 2009; Stift et al., 2013; Vieira et al., 2021). An interesting observation is that the phenotypes
356 on which the load was revealed varied among these studies. Here, the effect of homozygosity at the
357 *S*-locus was apparent on juvenile survival and on the length of the longest flowering stem, but we
358 detected no effect on any other morphological measurements, including leaf and rosette traits. In the
359 same population of *A. halleri,* Llaurens et al. (2009a) detected an effect on juvenile survival and on
360 leaf size. A study in North American outcrossing populations of *A. lyrate* (Stift et al., 2013) detected an
361 effect on juvenile survival, but not on any other traits that they measured. In the horsenettle *Solanum*
362 *carolinense*, the load was associated with reduced seed viability, flower number and germination
363 (Stone, 2004; Mena-Ali et al., 2009). Hence, the most consistent pattern seems to be a decrease of
364 overall juvenile survival, possibly because it is a highly integrative measurement of fitness, whereas
365 other morphological or life history traits can be associated with more specific components of overall
366 fitness.

367 *A unique genetic load associated with each allele in each population.*

368 The model of the sheltered load posits that each *S*-allele should be associated with a specific set of
369 linked mutations (Llaurens et al., 2009a). In line with this prediction, the magnitude of the *S*-linked
370 load varied among *S*-alleles, as the load linked to some *S*-alleles was phenotypically detectable, while
371 for others it was not. This variation of the genetic load is expected, since deleterious mutations
372 associated with the different alleles are likely to hit different linked genes, and affect different
373 phenotypic traits with different effects on fitness. Also in line with the model of the sheltered load,
374 our phasing of a large number of variants linked to *S*-haplotypes in several natural populations
375 revealed that the same suite of linked mutations was consistently associated among different copies
376 of a given *S*-allele when sampled from within the same population, in particular for the dominant *S*-
377 allele lineages under more intense balancing selection. As expected for outcrossing populations with
378 short-scale linkage disequilibrium, this association was lost when examining sites at increasing genetic
379 distances from the *S*-locus along the chromosome (see also Le Veve et al., 2023). Finally, the
380 association with linked sites was further lost when comparing gene copies of *S*-alleles sampled from
381 different local populations, suggesting that recombination within populations decouples alleles from
382 their linked sites faster than migration can homogenise the genetic composition among these natural
383 populations. We note that the patterns of association and phylogenetic structure differed among
384 populations, possibly due to their contrasted demographic histories. Indeed, the *A. lyrata* populations
385 colonised North America from ancestral European populations about 20-30.000 years ago (Clauss et
386 al., 2006; Ross-Ibarra et al., 2008), and are less diverse overall than the *A. halleri* populations we
387 studied, who colonised the north of France during the last century from ancestral German populations
388 (Pauwels et al., 2005). The progressive decoupling between alleles and their linked sites leads to the
389 simple prediction that *S*-locus homozygous genotypes formed by crossing individuals carrying identical
390 alleles from distinct populations should not reveal as much load as when they are formed by crossing
391 individuals within populations. Hence, the *S*-locus region could contribute to overall hybrid vigour.
392 Testing this prediction will be an interesting next step.

393 *Different properties of the linked load according to S-allele dominance*

394 The question of whether variations in the intensity of balancing selection, mediated by *S*-allele
395 dominance, could explain variation of the linked load has received conflicting support in the literature.
396 In line with Stift et al. (2013), but in contradiction with Llaurens et al. (2009a), we observed no overall
397 effect of dominance on the magnitude of the load. Several technical and biological reasons could
398 explain the contrasted results obtained in these different studies. First, phenotypic quantification of
399 the linked load is experimentally demanding, such that these studies relied on the comparison of a
400 limited number of alleles (three *S*-alleles in each of the studies) and therefore each of them had
401 inherently low power. Second, the experimental procedures to reveal the load varied slightly. Llaurens
402 et al. (2009a) used CO_2 treatment to by-pass the SI system and obtain homozygous progenies from
403 crosses that would otherwise have been incompatible, whereas we used the "natural" masking by
404 dominant *S*-alleles to enable the obtention of recessive homozygous genotypes. Our approach is
405 experimentally simpler and avoids the possible contamination by offspring obtained by selfing, which
406 may confound the effect of the sheltered load with that of genome-wide inbreeding depression (see
407 Stift et al., 2013 for a detailed discussion of this caveat). Third, a limitation of our approach is that it is
408 restricted to *S*-alleles that are recessive or intermediate along the dominance hierarchy, and is thus
409 not applicable to quantify the load associated with the most dominant *S*-alleles under more intense
410 balancing selection. It is therefore possible that the *S*-alleles we examined did not exhibit sufficiently
411 contrasted levels of dominance, in particular if only the most dominant ones are generating a
412 substantial load, as suggested for fully linked recessive deleterious mutations (Llaurens et al., 2009a).
413 In addition, since the homozygous *S*-allele genotypes we created correspond to different gene copies
414 from the population, they may carry distinct sets of linked variants, especially for the more recessive
415 *S*-alleles. The variation we observed in the phenotypic magnitude of the load among families confirms
416 that linked deleterious variants are unlikely to be fixed within all allele lineages. Finally, we note that
417 our genomic analysis of the genetic load shows that the dominant allele Ah15 previously associated
418 with reduced fitness in homozygotes (Llaurens et al., 2009a), is indeed unusual in terms of the number
419 of mutations it carries. In fact, it is one of the most "loaded" alleles among all the dominant *S*-alleles
420 present in this population, possibly explaining why Llaurens et al. (2009a) observed a significant effect
421 despite the inherently limited experimental power of their analysis.

422 A possible caveat of the population genetics approach we used is that simply counting up the number
423 of putatively deleterious linked mutations is a very crude estimate of the genetic load. We note that
424 our conclusions are robust to differences in the way we define deleterious mutations: as variants at
425 0-fold degenerate sites, at non-synonymous sites, or using methods to quantify the severity of
426 mutations such as SNPeff of SIFT4G. An obvious limitation is that none of these approaches allow for
427 evaluation of recessivity - a concept critical to ideas concerning the sheltered load. Our stochastic
428 simulations could be improved in several ways. First, we examined the accumulation of linked
429 deleterious mutations that were assumed to be fully recessive. This choice was guided by the
430 observation by Llaurens et al. (2009a) that fully recessive mutations accumulate more substantially,
431 but it remains possible that the dynamics of deleterious mutations that are only partially recessive
432 may involve a complex interaction with dominance of the S-alleles to which they are linked. Second,
433 allowing for partial recombination between S-alleles and their linked deleterious mutations in the
434 simulations would also be necessary to predict the length of the chromosomal haplotypes associated
435 with dominant vs. recessive *S*-alleles. In spite of these limitations, our stochastic simulations and
436 genomic analyses concur to the conclusion that the variation of the intensity of balancing selection
437 among *S*-alleles affect the genetic architecture of the linked load: a larger proportion of putatively

deleterious mutations are fixed among gene copies of the dominant as compared to the recessive *S*-alleles, while gene copies of the recessive *S*-alleles tend to accumulate more segregating deleterious variation. While these two processes eventually compensate one another, they may have distinct consequences for the evolution of *S*-alleles. Uyenoyama (2003) showed that the existence of a sheltered load should influence the evolutionary dynamics of new *S*-alleles through self-compatible intermediates. Specifically, antagonistic interactions are expected between ancestral and derived functional specificities because they would initially share their linked deleterious mutations, slowing down the establishment of new *S*-alleles. Our observation that partially different sets of linked mutations are associated with *S*-alleles from the different populations raises the question of whether the (short) time scale at which recombination decouples *S*-alleles from their sets of linked mutation is sufficiently fast to impede such antagonistic interactions to take place. In other words, the effect of the load on the diversification dynamics should be most important if the two mutational steps required for the emergence of new *S*-alleles under this model take place within local populations, rather than involving a metapopulation-scale process. As shown by Stetsenko et al. (2023), this is expected to occur under very low dispersal only. In addition, the observation that the architecture of the sheltered load differs between dominant and recessive *S*-alleles suggests that their diversification dynamics may also differ. Specifically, the self-compatible intermediates required for the formation of new *S*-alleles (Gervais et al., 2011; Bergero and Charlesworth, 2009) are expected to be capable of selfing as well as forming homozygous genotypes that would otherwise be prevented. While the consequences of selfing may be equivalent for all alleles (because the overall number of mutations to which they are linked are equivalent), the consequences of the formation of homozygotes allowed by the crossing of separate individuals sharing a given *S*-allele are expected to be more severe for dominant *S*-alleles. The segregation of distinct deleterious variants linked to different gene copies of recessive *S*-alleles implies that linked recessive deleterious mutations are likely to remain masked when two distinct gene copies of a given recessive *S*-allele are brought together. Hence, our results lead to the prediction that in natural populations self-compatible mutants may segregate more readily for the more recessive than for the more dominant *S*-alleles, and more generally for allelic lineages under lower intensity of balancing selection. Considering that self-compatible mutants are a necessary intermediate stage in the formation of new *S*-alleles, one may predict that the diversification dynamics should be more efficient for lineages of recessive than dominant *S*-alleles. This prediction is in line with the observation in Arabidopsis that the most dominant S-alleles exhibit the deepest phylogenetic divergence among them (Durand et al., 2014). Detailed quantification of the presence of self-compatible variants in natural populations will now be necessary to test this hypothesis. At this stage, however, a proper model of allelic diversification taking into account dominance interactions among *S*-alleles is still missing.

Variations of the genetic load among balanced allelic lines is a general phenomenon. The classical case of Y or W sex chromosomes are indeed examples where one balanced line accumulates a greater genetic load than the other (X or Z, respectively), eventually leading to substantial genetic degeneration (Wright et al., 2016; Ponnikas et al., 2018). Another example is the supergene controlling variation in male plumage phenotypes of the ruff, where the genetic load on the derived "Satellite" haplotype is higher than on the ancestral "Independent" haplotype (Lamichhaney et al., 2016; Hill et al., 2022). Similarly, in the butterfly *Heliconius numata*, the inverted haplotypes conferring mimetic wing patterns tend to accumulate a greater load than the non-inverted haplotypes (Rosser et

al., 2022). Interestingly, in all these cases, the haplotypes with the greatest load also act genetically in a dominant manner, establishing a clear parallel with our observations.

It is clear from our results that *S*-allele dominance affects the linked load, but in turn the differences in structure of the linked load may affect the conditions under which dominance can evolve. The Brassicaceae *S*-locus is a unique system, where dominance is controlled by "dominance modifiers" (Durand et al., 2014; Durand et al. 2020). The presence of deleterious mutations linked to *S*-alleles has been shown to affect the evolution of dominance modifiers, favouring evolution towards greater dominance than towards greater recessivity (Llaurens et al., 2009b). This asymmetry arises from the fact that *S*-alleles that become recessive (e.g. following acquisition of a recessivity modifier such as a small RNA target) will start forming homozygous genotypes, leading to expression of their linked load, while *S*-alleles that become dominant will not. Our observation that many deleterious mutations linked to recessive *S*-alleles are indeed segregating, suggests that expression of the load will be less severe for recessive than for dominant *S*-alleles, hence decreasing this predicted asymmetry. It will now be essential to modify models for the evolution of dominance to allow for such differential load among *S*-alleles.

497 ## Material and Methods

498 *Source plant material*

499 We worked on natural accessions from two closely related species, *A. halleri* and *A. lyrata*, represented
500 by two population samples named Mortagne (50°47'N, 3°47'E, France, *n*=60) and Nivelle (50°47'N,
501 3°47'E, France, *n*=61) for *A. halleri*, and three highly outcrossing population samples from the North
502 American Great Lakes, named IND (Indiana Dunes National Lakeshore in Michigan, *n*=9), PIN (Pinery
503 Provincial Park in Ontario, *n*=11) and TSS (Tobermory Provincial Park in Ontario, *n*=8; Foxe et al., 2010)
504 for *A. lyrata* (Fig. S9). The *A. lyrata* populations colonised North America from ancestral European
505 populations about 20-30.000 years ago (Clauss and Mitchell-Olds, 2006; Ross-Ibarra et al., 2008) and
506 the *A. halleri* populations are peripheral and likely colonised the north of France during the last century
507 from ancestral German populations (Pauwels et al., 2005).

508 We performed 92, 91, 40, 43 and 21 controlled crosses between randomly chosen individuals within
509 the Nivelle, Mortagne, IND, PIN and TSS populations, respectively. We successfully obtained seeds
510 from 60, 66, 21, 21 and 10 of these crosses, respectively. Because we were not interested in estimating
511 population frequencies of *S*-alleles, we instead tried to maximise the number of reconstructed
512 haplotypes and avoid over representing the most recessive *S*-allele (Ah01) that tends to segregate at
513 very high frequencies in natural populations (Llaurens et al., 2008). To do this, we performed PCR with
514 *S*-allele-specific primers (Llaurens et al., 2008; Goubet et al., 2012) to screen the parents of the crosses
515 and we removed from the experiment offspring with two parents carrying allele Ah01. For *A. halleri*,
516 we selected 19 individuals from the Nivelle population and 19 individuals from the Mortagne
517 population, based on their genotype at the *S*-locus (Fig. S9; Table S7). We also selected one offspring
518 of 9, 11, 5, 6 and 5 pairs of selected individuals in the Nivelle, Mortagne, IND, PIN and TSS populations
519 respectively for the phasing of *S*-haplotypes (Table S8; Fig. S9). To increase sample size for the
520 phenotypic measurements, we included offspring from five additional crosses from the Nivelle
521 population (Table S8).

522 *Library preparation, capture and sequencing*

523 We used a previously developed sequence capture approach to specifically sequence genomic regions
524 of interest (Le Veve et al., 2023). Briefly, indexed genomic libraries were constructed for each
525 individual and libraries were pooled in equimolar proportions. Fragments matching a series of regions
526 of interest (including in particular the 75kb upstream and downstream of the non-recombining *S*-locus
527 region as well as a series of 100 unlinked 25kb regions used as genomic controls; Le Veve et al., 2023),
528 were then enriched using synthetic 120bp RNA probes and sequenced by Illumina MiSeq (a total of
529 159 million paired-end reads).

530 For six individuals (Table S7, S8), we completed the sequencing with genome-wide resequencing
531 (WGS) in order to distinguish the homozygous and heterozygous genotypes at the *S*-locus based on
532 read depth (Genete et al., 2020), which is not possible using data from the capture protocol. The
533 prepared libraries were sequenced by Illumina NovaSeq (2x 150pb, paired-end) from the GenoScreen
534 platform (Lille, France).

535 *Determination of the S-locus genotypes and dominance of S-alleles*

536 We used a dedicated pipeline for genotyping the *S*-locus based on short reads sequencing (Genete et
537 al., 2020) obtained from each individual (Table S7 and S8). The level of dominance of *S*-alleles found
538 in our study was determined based on either previous assessment of dominance in *A. lyrata* and *A.*
539 *helleri* (Schierup et al., 2001; Mable et al., 2003; Bechsgaard,et al., 2004; Llaurens et al., 2008; Goubet
540 et al., 2012) or indirectly inferred based on the observed association between the phylogeny of *S*-
541 alleles and levels of dominance (Prigoda et al., 2005).

542 *Read mapping and variant calling in A. halleri and A. lyrata populations*

543 Raw reads were mapped on the complete *A. lyrata* reference genome V1.0.23 (Hu et al., 2011) using
544 Bowtie2 v2.4.1 (Langmead and Salzberg, 2012), as described in Le Veve et al. (2023). File formats were
545 then converted to BAM using samtools v1.3.1 (Li et al., 2009) and duplicated reads were removed with
546 the MarkDuplicates program of picard-tools v1.119 (http://broadinstitute.github.io/picard). These
547 steps were performed by the custom Python script sequencing_genome_vcf.py available at
548 https://github.com/leveveaudrey/analysis-of-polymorphism-S-locus.

549 We obtained an average of 620 million properly mapped paired-end 300bp reads per population
550 sample. For consistency, we conserved only reads which mapped to the *S*-locus flanking or control
551 regions, even for samples sequenced by WGS, using the *targetintercept* option of bedtool v2.25.0
552 (Quinlan and Hall, 2010). We called all SNPs within the chromosomal segment comprising 50 kb
553 upstream from the first base of the gene *Ubox* in 3' and 50 kb downstream from the last base of the
554 gene *ARK3* in 5' of the *S*-locus using the Genome Analysis Toolkit v. 3.8 (GATK; DePristo et al., 2011)
555 with the option GVCF and a quality score threshold of 60 using vcftool v0.1.15 (Danecek et al., 2011).
556 This region contains 20 annotated protein-coding genes. In this study we excluded the genes inside
557 the *S*-locus itself (*SCR*, *SRK*). For each sample independently, we computed the distribution of coverage
558 depth across control regions using samtools depth (Li et al., 2009). We excluded sites with either less
559 than 15 reads aligned or coverage depth above the 97.5 % percentile, as the latter are likely to
560 correspond to repeated sequences (e.g. transposable elements or paralogs). Finally, we removed SNPs
561 fixed in each population using the script 1_fix_pos_vcf.py
562 (https://github.com/leveveaudrey/dominance_and_sheltered_load), thus retaining only nucleotide
563 sites that were variable in the population.

564 *Quantifying the sheltered load of deleterious mutations*

565 We examined deleterious mutations based on the accumulation of either 1) mutations on 0-fold
566 degenerate sites, 2) all non-synonymous mutations, 3) mutations predicted to be deleterious based
567 on the SIFT4G database (Vaser et al,. 2016) or 4) mutations predicted to be lowly, moderately and
568 highly deleterious by SNPeff (Cingolani et al,. 2012). The 0-fold and 4-fold degenerate sites were
569 identified and extracted from the reference genome and the gene annotation using the script
570 NewAnnotateRef.py (Williamson et al., 2014). None of the tools used to predict deleterious mutations
571 are able to determine dominance levels of the mutation. Thus, all the deleterious mutations were
572 considered as recessive. Details of the number of deleterious for each type is presented in Table S6.

573 *Phasing S-haplotypes*

574 For each of the 9, 11, 5, 6 and 5 trios analysed in the Nivelle, Mortagne, IND, PIN and TSS populations
575 respectively, we phased mutations in the flanking regions, resulting in 130 phased haplotypes (Fig.
576 S9). Briefly, we used sites that were heterozygous in the offspring to resolve parental haplotypes by
577 assuming no recombination between parent and offspring, thus attributing the allelic state that was
578 shared between a parent and its offspring to their shared *S*-allele, and the allelic state that was not
579 shared to the other (untransmitted) haplotype of the parent. Twelve of the parents had been used in
580 more than one cross, and in these cases we phased their haplotypes only once (Table S8). We
581 implemented the phasing procedure in the script 3_phase_S_allele.py available at
582 https://github.com/leveveaudrey/dominance_and_sheltered_load.

583 *Study of the structure of S-haplotypes*

584 We first developed a new method to evaluate the distortion of the phylogenetic patterns caused by
585 linkage to *S*-alleles. To do this, we used phyml v.3.3 (Guindon et al., 2010) to calculate the likelihood

586 of two contrasted topologies of interest: (1) the topology clustering haplotypes by the populations
587 where they came from vs. (2) the topology clustering them by the *S*-allele to which they are linked (Fig
588 2A). We used sliding windows of sequences with 50 SNPs to obtain the variation of the difference in
589 log-likelihood between these two topologies along the chromosome. We then compared these values
590 to their distribution throughout the genome obtained by random draws of sequences with 50 SNPs
591 from the control regions. Second, we visualised the relationships among the phased haplotypes using
592 maximum likelihood phylogenies based on the Tamura-Nei model (Tamura and Nei, 1993), with 1,000
593 replicates in MEGA X (Kumar et al., 2018). Third, we followed Kamau et al.'s (2007) approach and
594 examined the variation of F_{ST} among populations within each species (Nivelle and Mortagne for *A.*
595 *halleri* and IND, PIN and TSS for *A. lyrata*) along the flanking region in non-overlapping windows of
596 5kb. We also examined the variation of F_{ST} along the flanking region obtained by grouping haplotypes
597 by their linked *S*-allele rather than by population of origin. Then, we compared these F_{ST} values
598 computed in the *S*-locus flanking regions with their genomic distribution as determined from the 100
599 control regions. The F_{ST} values were estimated with the DNAsp 6 software (Rozas et al., 2017). Fourth,
600 we performed a major component analysis (MCA) based on SNPs in the first 5kb, SNPs between 5 and
601 25kb and SNPs between 25 and 50kb around the *S*-locus, using the R packages 'ggplot2' (version 3.4.0),
602 'factoextra' (version 1.0.7) and 'FactoMiner' (version 2.7). We compared the patterns obtained by
603 these MCAs with those obtained from identical numbers of SNP (+/- 1%) from the control regions.
604 Finally, we analysed genetic association in each population independently between each of the locally
605 segregating variants and the *S*-alleles considered as phenotypes, using STRAT V1.1 (Pritchard et al.,
606 2000) combined with Structure V2.3 (Pritchard et al., 2010). We examined the distribution of the top
607 0.1% most significant associations detected specifically for each *S*-allele in each population.

608 *Estimation of the number of fixed and segregating deleterious mutations within S-allele lineages*

609 For each variable position considered in the phased haplotypes, we estimated the number of
610 mutations on 0-fold (S_{0f}) and 4-fold degenerate sites (S_{4f}) compared with the reference genome. We
611 distinguished SNPs that were fixed from those that were segregating within each of the allelic lines.
612 We used GLM with a Poisson distribution to test whether the number of fixed and segregating
613 mutations were associated with *S*-allele dominance, considering populations as random effects. The
614 dominance of the S-allele was considered a continuous variable. We reiterated the GLM analysis with
615 the number of non-synonymous (S_{NS}), synonymous (S_S), lowly and moderately deleterious mutations
616 predicted by SNPeff and deleterious mutations predicted by SIFT4G mutations.

617 *Estimation of the phenotypic impact of homozygosity at the S-locus for three S-alleles*

618 To determine if the genetic sheltered load putatively linked to the *S*-locus has a detectable phenotypic
619 impact, we performed 45 crosses (Table S1) between offspring of the Nivelle individuals that we chose
620 so that they shared one *S*-allele (Fig. S9). Based on the dominance hierarchy in pollen (Durand et al.,
621 2014; Table S1), these crosses should correspond to compatible partners. The general principle of the
622 experiment was to take advantage of the dominance hierarchy to mask recessive *S*-alleles and
623 generate full sibs that were either homozygous (because they inherited the *S*-allele that was shared
624 by their two parents) or heterozygous at the *S*-locus, and thus isolate the effect of homozygosity at
625 the *S*-locus. Note that all offspring in our experiments were thus "naturally" outcrossed, whereas
626 Llaurens et al. (2009a) based their comparisons on outcrossed progenies obtained by enforced
627 incompatible crosses and Stift et al.[19] based their comparisons on enforced selfed progenies. These
628 crosses generated 399 seeds overall, with homozygous genotypes expected for the *S*-alleles Ah01,
629 Ah03 and Ah04 forming the following dominance relationship: Ah01<Ah03<Ah04.

630 Seedlings were grown in a greenhouse between 14.5 and 23.1°C and a photoperiod of 16 hr day/8 hr
631 night. Offspring from the six families were placed on tables, and their position randomised every three
632 days. After three months of growing, all the germinated plants were vernalised under a temperature
633 between 6 and 8°C and a natural photoperiod for two months (January-February). Then, all surviving

634 plants began reproduction in a greenhouse under temperature between 10.6 and 25.3°C and a natural
635 photoperiod. The genotypes at the *S*-locus were determined in surviving plants by a PCR approach,
636 using *S*-allele-specific primers for the pistil-expressed *SRK* gene. We assessed the reproductive success
637 of offspring from the different crosses on the basis of fourteen phenotypic traits (detailed below) and
638 computed the mean difference for the trait between homozygotes and heterozygotes within each
639 family. We also tested for departures from mendelian proportions of each *S*-locus genotypic category
640 in the family after the apparition of the first stem. Significant departures were interpreted as reflecting
641 differences in survival between homozygous and heterozygous *S*-locus genotypes. We performed
642 10,000 replicate simulations of mendelian segregation based on the *S*-locus genotype of the parents.
643 We used GLM to test whether the phenotypic impact of homozygosity at the *S*-locus increased with
644 dominance of the *S*-alleles, considered as a continuous variable. The models used for GLM depended
645 on the type of trait analysed (poisson for the counts like the number of leaves, flowers by stems or
646 days; gaussian for continue traits like the lengths, widths and areas).

647 We measured the following fourteen phenotypic traits: the time (days) to the first leaf measured by
648 visual control every day during seven weeks after sowing the seeds, the number of leaves, the area of
649 the rosette (cm^2), the mean length and width of leaves (cm), the standard deviation of length and
650 width of leaves (cm) and the mean area of leaves (cm^2) measured by ImageJ (Schneider et al., 2012)
651 based on photographs taken seven weeks (+/- five days) after the first leaf. At reproduction, we
652 measured the time to the first flower bud for the end of vernalisation (day), scored by visual control
653 every three days during nine weeks, the number of flower buds per flower stem produced during four
654 week after the appearance of the first bud, the number of flower stems, the length of the highest
655 flower stem produced four weeks after the appearance of the first bud (cm), and finally the total
656 duration of buds production (days), scored by visual control every three days during eleven weeks
657 after the appearance of the first bud. The last trait we measured was the proportion of homozygotes
658 per family that survived until reproduction assuming mendelian proportions in the seeds. During the
659 whole experiment, the presence of phytophagous insects, pathogens and stress markers were scored
660 as binary variables. The presence of phytophagous insects and pathogen attacks were detected by the
661 occurrence of gaps in leaves. Oxidative stress was scored qualitatively based on the occurrence of
662 purple leaves. We also controlled the effect of the family on the phenotypic trait. These effects were
663 controlled by redistributing 10,000 times the values observed in groups of the same size observed for
664 each effect (for example, presence or absence of pathogen attack) and comparing the difference for
665 the trait observed with the distribution of the differences obtained in the permutations. We
666 considered the impact of the effect on the trait if the observed difference between groups was higher
667 than the 95% percentile of the distribution obtained randomly (Table S9). When the test was
668 significant, the effect was implemented as a random effect in the GLM. We used the same method to
669 control for the family effect, which was included as a random effect in GLM if necessary (Table S10).
670 The general experimental procedure is summarised in Fig. S9 and all data analyses were done in R ver.
671 3.1.2 (R Development Core Team 2014).

672 *Simulations*

673 Finally, we refined the model of Llaurens et al. (2009a), in several ways. We simulated a panmictic
674 population of *N* diploid individuals with non-overlapping generations. Each individual was defined by
675 its genotype in a non-recombining genomic region. This region contains the *S*- locus, and a D locus
676 where deleterious mutations accumulated. For the *S*-locus, we used a simple model of sporophytic SI,
677 with four dominance classes, as observed in *A. halleri* (Genete et al., 2020; only three classes were
678 considered before in Llaurens et al., 2009a), and fourteen *S*-alleles (eight alleles in the class IV, three
679 in the class III, two in the class II and one allele in the class I). This distribution mirrors that of the
680 Nivelle population (Table S7), with the exception that a class II allele has been added because its
681 presence has been reported in previous studies (Llaurens et al., 2008). Alleles within classes were
682 assumed to be codominant with each other, and dominant over all alleles of the more recessive
683 classes, with the following linear hierarchy between classes : classI<classII<classIII<classIV). We also

assumed that no new *S*-allele could appear by mutation during the simulations. The population size was 10,000 diploid individuals, so as to be large enough to avoid *S*-allele loss by drift during the simulations (previously it was 1,000). The "D locus" comprised one hundred fully linked biallelic positions (versus a single one in Llaurens et al., 2009a). Fully recessive deleterious mutations were recurrently introduced (at a rate 10^{-4}), and reverse mutations were possible (at a rate 10^{-5}). We ignored partially recessive deleterious mutations because these mutations were predicted to be effectively eliminated by natural selection in Llaurens et al. (2009a). The survival probability p of a zygote depended on its genotype at the D locus: $p = (1 - s)^n$ with s the selection coefficient and n the number of positions homozygous for the mutated allele. We explored different values of the selection coefficient (0.1, 0.05, 0.03, 0.01 and 0.005). Under strong selection (s=0.1, 0.05 and 0.03), the combined effect of multiple mutations led to low-fitness individuals, eventually causing population extinction. Under weak selection, (s=0.005), we observed near fixation of the deleterious mutations under the influence of asymmetrical mutation. Hence, we focused on the intermediate value of the selection coefficient (s=0.01), where deleterious mutations segregated stably in the simulations.

We first ran simulations without deleterious mutations until a deterministic equilibrium for *S*-allele frequencies was reached, which was considered to be attained when allelic frequencies changed by less than 10^{-3} between generations. Recessive deleterious mutations were then allowed to accumulate at the positions within the D locus. Each simulation was performed with 100 independent replicates of 100,000 generations, and the frequency of the deleterious alleles was recorded every 1,000 generations. At the end of the simulation runs, we estimated the number of deleterious mutations found in each haplotype associated with each *S*-allele to determine the expected patterns of association between the sheltered load and dominance at the *S*-locus.

The code of the program of simulations developed in Llaurens et al. (2009a) and used in our study is available in Github (https://github.com/leveveaudrey/model_ssi_Llaurens).

Data Availability

All sequence data are available in the NCBI Short Read Archive (SRA; https://www.ncbi.nlm.nih.gov/sra) with accession codes: PRJNA744343, PRJNA755829.

All scripts developed are available in Github (https://github.com/leveveaudrey/dominance_and_sheltered_load https://github.com/leveveaudrey/analysis-of-polymorphism-S-locus).

The code of the program of simulations developed in Llaurens et al. (2009a) and used in our study is available in Github (https://github.com/leveveaudrey/model_ssi_Llaurens).

Acknowledgements

This work was funded by the European Research Council (NOVEL project, grant #648321) and ANR TE-MoMa (grant ANR-18-CE02-0020-01). AL's PhD thesis was funded by the ERC and the University of Lille. The authors thank Barbara Mable for sharing seeds of *A. lyrata* and Camille Roux for discussions. This work was performed using infrastructure and technical support of the Plateforme Serre, cultures et terrains expérimentaux - Université de Lille for the greenhouse/field facilities. The authors thank the UMR 8199 LIGAN-MP Genomics platform (Lille, France) which belongs to the 'Federation de Recherche' 3508 Labex EGID (European Genomics Institute for Diabetes; ANR-10-LABX-46) and was supported by the ANR Equipex 2010 session (ANR-10-EQPX-07-01; 'LIGAN-MP'). The LIGAN-MP Genomics platform (Lille, France) is also supported by the FEDER and the Region des Hauts-de-France. The authors thank the GenoScreen platform (Lille, France).

Author contributions

728 AL, ED, VC and XV developed and designed the experiments for the study. AL, CBL and CP performed
729 the experiments. AL and MG analysed and interpreted the data. AL, ED, VC and XV wrote the
730 manuscript. All authors edited the manuscript.

731 Declaration of interests

732 The authors declare no competing interests.

733 References

734 Bechsgaard J, Bataillon T, and Schierup M.H (2004) Uneven segregation of sporophytic self-
735 incompatibility alleles in *Arabidopsis lyrata*. Journal of Evolutionary Biology 17, 554–561.
736 https://doi.org/10.1111/j.1420-9101.2004.00699.x.

737 Bergero R, and Charlesworth D (2009) The evolution of restricted recombination in sex chromosomes.
738 Trends in Ecology & Evolution 24, 94–102. https://doi.org/10.1016/j.tree.2008.09.010.

739 Billiard S, Castric V, and Vekemans X (2007) A general model to explore complex dominance patterns
740 in plant sporophytic self-incompatibility systems. Genetics 175, 1351–1369.
741 https://doi.org/10.1534/genetics.105.055095

742 Castric V, and Vekemans X (2004) Plant self-incompatibility in natural populations: a critical
743 assessment of recent theoretical and empirical advances. Molecular Ecology 13, 2873–
744 2889.https://doi.org/10.1111/j.1365-294X.2004.02267.x.

745 Charlesworth D (2006) Balancing selection and its effects on sequences in nearby genome regions.
746 PLOS Genetics 2, e64. https://doi.org/10.1371/journal.pgen.0020064.

747 Cingolani, P., Platts, A., Wang, L.L., Coon, M., Nguyen, T., Wang, L., Land, S.J., Lu, X., Ruden, D.M., 2012.
748 A program for annotating and predicting the effects of single nucleotide polymorphisms, SnpEff. Fly
749 (Austin) 6, 80–92. https://doi.org/10.4161/fly.19695

750 Clauss M.J, and Mitchell-Olds T (2006) Population genetic structure of *Arabidopsis lyrata* in Europe.
751 Molecular Ecology 15, 2753–2766. https://doi.org/10.1111/j.1365-294X.2006.02973.x.

752 Cocker J.M, Wright J, Li J, Swarbreck D, Dyer S, Caccamo M, and Gilmartin P.M (2018) *Primula vulgaris*
753 (primrose) genome assembly, annotation and gene expression, with comparative genomics on the
754 heterostyly supergene. Sci Rep 8, 17942. https://doi.org/10.1038/s41598-018-36304-4.

755 Danecek P, Auton A, Abecasis G, Albers C.A, Banks E, DePristo M.A, Handsaker R.E, Lunter G, Marth
756 G.T, Sherry S.T, et al (2011) The variant call format and VCFtools. Bioinformatics 27, 2156–2158.
757 https://doi.org/10.1093/bioinformatics/btr330.

758 DePristo M.A, Banks E, Poplin R.E, Garimella K.V, Maguire J.R, Hartl C, Philippakis A.A, del Angel G,
759 Rivas M.A, Hanna M, et al (2011) A framework for variation discovery and genotyping using next-
760 generation DNA sequencing data. Nat Genet 43, 491–498. https://doi.org/10.1038/ng.806.

761 Durand E, Méheust R, Soucaze M, Goubet P.M, Gallina S, Poux C, Fobis-Loisy I, Guillon E, Gaude T,
762 Sarazin A, et al (2014) Dominance hierarchy arising from the evolution of a complex small RNA
763 regulatory network. Science 346, 1200–1205. https://doi.org/10.1111/eva.12933.

764 Durand E, Chantreau M, Le Veve A, et al (2020) Evolution of self-incompatibility in the Brassicaceae:
765 Lessons from a textbook example of natural selection. Evolutionary Applications.
766 https://doi.org/10.1111/eva.12933.

767 Foxe J.P, Stift M, Tedder A, Haudry A, Wright S.I, and Mable B.K (2010) Reconstructing origins of loss
768 of self-incompatibility and selfing in North american *Arabidopsis lyrata*: a population genetic context.
769 Evolution 64, 3495–3510. https://doi.org/10.1111/j.1558-5646.2010.01094.x.

770 Genete M, Castric V, and Vekemans X (2020) Genotyping and *de novo* discovery of allelic variants at
771 the Brassicaceae self-incompatibility locus from short read sequencing data. Mol Biol Evol.
772 https://doi.org/10.1093/molbev/msz258.

773 Gervais C.E, Castric V, Ressayre A, and Billiard S (2011) Origin and diversification dynamics of self-
774 Incompatibility haplotypes. Genetics 188, 625–636. https://doi.org/10.1534/genetics.111.127399.

775 Goubet P.M, Bergès H, Bellec A, Prat E, Helmstetter N, Mangenot S, Gallina S, Holl A.-C, Fobis-Loisy I,
776 Vekemans X, et al (2012) Contrasted patterns of molecular evolution in dominant and recessive self-
777 incompatibility haplotypes in Arabidopsis. PLoS Genetics 8, e1002495.
778 https://doi.org/10.1371/journal.pgen.1002495.

779 Guindon S, Dufayard J-F, Lefort V, et al (2010) New algorithms and methods to estimate maximum-
780 likelihood phylogenies: assessing the performance of PhyML 3.0. Syst Biol 59, 307–321.
781 https://doi.org/10.1093/sysbio/syq010.

782 Hartmann F.E, Duhamel M, Carpentier F, et al (2021) Recombination suppression and evolutionary
783 strata around mating-type loci in fungi: documenting patterns and understanding evolutionary and
784 mechanistic causes. New Phytologist 229:2470–2491. https://doi.org/10.1111/nph.17039.

785 Hatakeyama K, Watanabe M, Takasaki T, Ojima K, Hinata K. (1998). Dominance relationships between
786 S -alleles in self-incompatible Brassica campestris L. Heredity 80, 241–247.
787 https://doi.org/10.1046/j.1365-2540.1998.00295.x

788 Hill J, Enbody E, Bi H, Lamichhaney S, Schwochow D, Younis S, Widemo F, and Andersson L (2022) Low
789 mutation load in a supergene underpinning alternative male mating strategies in ruff.
790 https://doi.org/10.1101/2022.04.27.489720.

791 Hu T.T, Pattyn P, Bakker E.G, Cao J, Cheng J.-F, Clark R.M, Fahlgren N, Fawcett J.A, Grimwood J,
792 Gundlach H, et al (2011) The *Arabidopsis lyrata* genome sequence and the basis of rapid genome size
793 change. Nat Genet 43, 476–481. https://doi.org/10.1038/ng.807.

794 Jay P, Chouteau M, Whibley A, Bastide H, Parrinello H, Llaurens V, and Joron M (2021) Mutation load
795 at a mimicry supergene sheds new light on the evolution of inversion polymorphisms. Nat Genet 53,
796 288–293. https://doi.org/10.1038/s41588-020-00771-1.

797 Jay P, Tezenas E, Véber A, and Giraud T (2022) Sheltering of deleterious mutations explains the
798 stepwise extension of recombination suppression on sex chromosomes and other supergenes. PLOS
799 Biology 20, e3001698. https://doi.org/10.1371/journal.pbio.3001698

800 Kakizaki T, Takada Y, Ito A, Suzuki G, Shiba H, Takayama S, Isogai A, Watanabe M. (2003). Linear
801 Dominance Relationship among Four Class-II S Haplotypes in Pollen is Determined by the Expression
802 of SP11 in Brassica Self-Incompatibility. Plant and Cell Physiology 44, 70–75.
803 https://doi.org/10.1093/pcp/pcg009

804 Kamau E, Charlesworth B, Charlesworth D (2007) Linkage Disequilibrium and Recombination Rate
805 Estimates in the Self-Incompatibility Region of Arabidopsis lyrata. Genetics 176, 2357–2369.
806 https://doi.org/10.1534/genetics.107.072231

807 Katsura Y, Iwase M, Satta Y (2012) Evolution of genomic structures on mammalian sex chromosomes.
808 Current Genomics 13:115–123. https://doi.org/10.2174/138920212799860625.

809 Kumar S, Stecher G, Li M, Knyaz C, and Tamura K (2018) MEGA X: Molecular evolutionary genetics
810 analysis across computing platforms. Molecular Biology and Evolution 35:1547-1549.
811 https://doi.org/10.1093/molbev/msy096.

812 Kusaba M, Dwyer K, Hendershot J, Vrebalov J, Nasrallah J.B, and Nasrallah M.E (2001) Self-
813 incompatibility in the genus Arabidopsis: characterization of the S locus in the outcrossing *A. lyrata*
814 and its autogamous relative *A. thaliana*. Plant Cell 13, 627–643.

815 Lamichhaney S, Fan G, Widemo F, Gunnarsson U, Thalmann D.S, Hoeppner M.P, Kerje S, Gustafson U,
816 Shi C, Zhang H, Chen W, Liang X, Huang L, Wang J, Liang E, Wu Q, Lee S.M.-Y, Xu X, Höglund J, Liu X,
817 and Andersson L (2016) Structural genomic changes underlie alternative reproductive strategies in the
818 ruff (*Philomachus pugnax*). Nat Genet 48, 84–88. https://doi.org/10.1038/ng.3430.

819 Lane M.D, and Lawrence M.J (1995) The population genetics of the self-incompatibility polymorphism
820 in *Papaver rhoeas*. X. An association between incompatibility genotype and seed dormancy. Heredity
821 75, 92–97. https://doi.org/10.1038/hdy.1995.108.

822 Langmead B, and Salzberg S.L (2012) Fast gapped-read alignment with Bowtie 2. Nat Methods 9, 357–
823 359. https://doi.org/10.1038/nmeth.1923.

824 Le Veve A, Burghgraeve N, Genete M, et al (2023) Long-term balancing selection and the genetic load
825 linked to the self-incompatibility locus in *Arabidopsis halleri* and *A. lyrata*. Molecular Biology and
826 Evolution msad120. https://doi.org/10.1093/molbev/msad120.

827 Li H, Handsaker B, Wysoker A, Fennell T, Ruan J, Homer N, Marth G, Abecasis G, Durbin R, and 1000
828 Genome Project Data Processing Subgroup (2009) The Sequence Alignment/Map format and
829 SAMtools. Bioinformatics 25, 2078–2079. https://doi.org/10.1093/bioinformatics/btp352.

830 Llaurens V, Billiard S, Leducq J.-B, Castric V, Klein E.K, and Vekemans X (2008) Does frequency-
831 dependent selection with complex dominance interactions accurately predict allelic frequencies at the
832 self-incompatibility locus in *Arabidopsis halleri* ? Evolution 62, 2545–2557.
833 https://doi.org/10.1111/j.1558-5646.2008.00469.x.

834 Llaurens V, Gonthier L, and Billiard S (2009a) The sheltered genetic load linked to the S locus in plants:
835 new insights from theoretical and empirical approaches in sporophytic self-incompatibility. Genetics
836 183, 1105–1118. https://doi.org/10.1534/genetics.109.102707.

837 Llaurens V, Billiard S, Castric V, and Vekemans X (2009b) Evolution of dominance in sporophytic self-
838 incompatibility systems: I. Genetic load and coevolution of levels of dominance in pollen and pistil.
839 Evolution 63, 2427–2437. https://doi.org/10.1111/j.1558-5646.2009.00709.x.

840 Mable B.K, Schierup M.H, and Charlesworth D (2003) Estimating the number, frequency, and
841 dominance of S -alleles in a natural population of *Arabidopsis lyrata* (Brassicaceae) with sporophytic
842 control of self-incompatibility. Heredity 90, 422–431. https://doi.org/10.1038/sj.hdy.6800261.

843 Mattila T.M, Laenen B, Horvath R, Hämälä T, Savolainen O, and Slotte T. (2019) Impact of demography
844 on linked selection in two outcrossing Brassicaceae species. Ecology and Evolution 9, 9532–9545.
845 https://doi.org/10.1002/ece3.5463

846 Mena-Ali J. I, Keser L. H, Stephenson A. G (2009) The effect of sheltered load on reproduction in
847 *Solanum carolinense*, a species with variable self-incompatibility. Sex. Plant Reprod. 22 63–67.
848 https://doi.org/10.1007/s00497-008-0092-x.

849 Nettancourt D (2001) Incompatibility and incongruity in wild and cultivated plants. (2nd ed. Springer-
850 Verlag, Berlin Heidelberg).

851 Pauwels M, Saumitou-Laprade P, Holl A.C, Petit D, and Bonnin I (2005) Multiple origin of metallicolous
852 populations of the pseudometallophyte *Arabidopsis halleri* (Brassicaceae) in central Europe: the
853 cpDNA testimony. Molecular Ecology 14, 4403–4414. https://doi.org/10.1111/j.1365-
854 294X.2005.02739.x.

855 Ponnikas S, Sigeman H, Abbott J.K, and Hansson B (2018) Why do sex chromosomes stop recombining?
856 Trends Genet 34, 492–503. https://doi.org/10.1016/j.tig.2018.04.001.

857 Prigoda N.L, Nassuth A, and Mable B.K (2005) Phenotypic and genotypic expression of self-
858 incompatibility haplotypes in *Arabidopsis lyrata* suggests unique origin of alleles in different
859 dominance classes. Molecular Biology and Evolution 22, 1609–1620.
860 https://doi.org/10.1093/molbev/msi153.

861 Pritchard J. K, Stephens M, Rosenberg N. A, and Donnelly P (2000) Association mapping in structured
862 populations. The American Journal of Human Genetics 67:170–181. https://doi.org/10.1086/302959.

863 Pritchard J. K, Wen X, & Falush D (2010) Documentation for structure software: Version 2.3. University
864 of Chicago, Chicago, IL, 1-37.

865 Quinlan A.R, and Hall I.M (2010) BEDTools: a flexible suite of utilities for comparing genomic features.
866 Bioinformatics 26, 841–842. https://doi.org/10.1093/bioinformatics/btq033.

867 Ross-Ibarra J, Wright S.I, Foxe J.P, Kawabe A, DeRose-Wilson L, Gos G, Charlesworth D, and Gaut B.S
868 (2008) Patterns of polymorphism and demographic history in natural populations of *Arabidopsis*
869 *lyrata*. PLOS ONE 3, e2411. https://doi.org/10.1371/journal.pone.0002411.

870 Rosser N, Edelman N.B, Queste L.M, et al (2022) Complex basis of hybrid female sterility and Haldane's
871 rule in Heliconius butterflies: Z-linkage and epistasis. Molecular Ecology 31:959–977.
872 https://doi.org/10.1111/mec.16272.

873 Rozas J, Ferrer-Mata A, Sánchez-DelBarrio J.C, Guirao-Rico S, Librado P, Ramos-Onsins S.E, and
874 Sánchez-Gracia A (2017) DnaSP 6: DNA sequence polymorphism analysis of large data sets. Molecular
875 Biology and Evolution 34, 3299–3302. https://doi.org/10.1093/molbev/msx248.

876 Schierup M.H, Mikkelsen A.M, and Hein J (2001) Recombination, balancing selection and phylogenies
877 in *MHC* and self-incompatibility genes. Genetics 159, 1833–1844.
878 https://doi.org/10.1093/genetics/159.4.1833

879 Schneider C.A, Rasband W.S, and Eliceiri K.W (2012) NIH Image to ImageJ: 25 years of image analysis.
880 Nat Methods 9, 671–675. https://doi.org/10.1038/nmeth.2089.

881 Schopfer C.R, Nasrallah M.E, and Nasrallah J.B (1999) The male determinant of self-incompatibility in
882 Brassica. Science 286, 1697–1700. https://doi.org/10.1126/science.286.5445.1697.

883 Stetsenko R, Brom T, Castric V, and Billiard S (2023) Balancing selection and the crossing of fitness
884 valleys in structured populations: diversification in the gametophytic self-incompatibility system.
885 Evolution 77:907–920. https://doi.org/10.1093/evolut/qpac065

886 Stift M, Hunter B.D, Shaw B, Adam A, Hoebe P.N, and Mable B.K (2013) Inbreeding depression in self-
887 incompatible North-American *Arabidopsis lyrata*: disentangling genomic and S-locus-specific genetic
888 load. Heredity 110, 19–28. https://doi.org/10.1038/hdy.2012.49.

889 Stone J.L (2004) Sheltered load associated with S-alleles in *Solanum carolinense*. Heredity 92, 335–
890 342. https://doi.org/10.1038/sj.hdy.6800425.

891 Tamura K, and Nei M (1993) Estimation of the number of nucleotide substitutions in the control region
892 of mitochondrial DNA in humans and chimpanzees. Molecular Biology and Evolution 10, 512–526.
893 https://doi.org/10.1093/oxfordjournals.molbev.a040023.

894 Uyenoyama M.K (1997) Genealogical structure among alleles regulating self-incompatibility in natural
895 populations of flowering plants. Genetics 147, 1389–1400.
896 https://doi.org/10.1093/genetics/147.3.1389.

897 Uyenoyama M.K (2003) Genealogy-dependent variation in viability among self-incompatibility
898 genotypes. Theoretical Population Biology 63, 281–293. https://doi.org/10.1016/S0040-
899 5809(03)00020-0.

900 Uyenoyama M.K (2005) Evolution under tight linkage to mating type. New Phytol. 165: 63–70.
901 https://doi.org/10.1111/j.1469-8137.2004.01246.x.

902 Vaser R, Adusumalli S, Leng S.N, Sikic M, Ng P.C. (2016). SIFT missense predictions for genomes. Nat
903 Protoc 11, 1–9. https://doi.org/10.1038/nprot.2015.123

904 Vieira J, Pimenta J, Gomes A, Laia J, Rocha S, Heitzler P, and Vieira C.P (2021) The identification of the
905 Rosa S-locus and implications on the evolution of the Rosaceae gametophytic self-incompatibility
906 systems. Sci Rep 11, 3710. https://doi.org/10.1038/s41598-021-83243-8.

907 Williamson R.J, Josephs E.B, Platts A.E, Hazzouri K.M, Haudry A, Blanchette M, and Wright S.I (2014)
908 Evidence for widespread positive and negative selection in coding and conserved noncoding regions
909 of *Capsella grandiflora*. PLOS Genetics 10, e1004622. https://doi.org/10.1371/journal.pgen.1004622.

910 Wright A.E, Dean R, Zimmer F, and Mank J.E (2016) How to make a sex chromosome. Nat Commun 7,
911 12087. https://doi.org/10.1038/ncomms12087.

912 Yasuda S, Wada Y, Kakizaki T, Tarutani Y, Miura-Uno E, Murase K, Fujii S, Hioki T, Shimoda T, Takada Y,
913 Shiba H, Takasaki-Yasuda T, Suzuki G, Watanabe M, Takayama S. (2017). A complex dominance
914 hierarchy is controlled by polymorphism of small RNAs and their targets. Nature Plants 3.
915 https://doi.org/10.1038/nplants.2016.206

916 ***Figures legend***

917 ***Figure 1: Effect of homozygosity at the S-locus on 13 phenotypic traits compared to heterozygotes.***
918 *For each trait, the phenotypic values in homozygotes (in grey) were normalised relative to the mean*
919 *phenotypic values in heterozygotes (in black). The distributions were obtained by 10,000 random*
920 *permutations. SD: Standard Deviation.*

921 ***Figure 2: Linkage to the S-locus locally distorts the phylogenetic relationships.*** *A. The two topologies*
922 *of interest cluster haplotypes either by the S-allele to which they are linked (top) or by the populations*
923 *where they came (bottom). Different S-alleles are represented by symbols of different colours, different*
924 *populations of origin are represented by symbols of different shapes. B. Difference in log likelihood of*
925 *the two topologies of interest. Dots correspond to the difference in log likelihood for overlapping series*
926 *of 50 SNPs around the S-locus for A. halleri (top panel) and A. lyrata (bottom panel). Positive values*
927 *correspond to chromosomal positions where the topology by S-alleles explains the phylogeny of*
928 *haplotypes better than the topology by populations. The right panels show the difference in log*
929 *likelihood in the control regions. 2.5 and 97.5 percentiles of the distribution in the control regions are*
930 *indicated by dashed lines.*

931 ***Figure 3: No overall effect of S-allele dominance on the total number of 0-fold degenerate mutations***
932 ***(S_{0f}) in the linked genomic regions within 25kb.*** *Each dot represents the mean number of mutations*
933 *observed among haplotypes linked to one S-allele in one population. The correlations evaluated by a*
934 *GLM are represented by lines, with confidence intervals represented in grey. The dominance was*
935 *considered a continuous variable. A: A. halleri. Black dots correspond to the Nivelle population, grey*
936 *dots to the Mortagne population. The red arrow points to the copy of Ah15, corresponding to the S-*
937 *allele whose sheltered load was phenotypically characterised by Llaurens et al. (2009a) in Nivelle. B: A.*
938 *lyrata. Red dots correspond to the IND population, black dots to the PIN population and blue dots to*
939 *the TSS population.*

940 ***Figure 4: The number of 0-fold degenerate mutations fixed in the 25kb regions flanking the S-locus***
941 ***increases with dominance of the S-allele associated.*** *Each dot represents the value obtained for*
942 *haplotypes linked to one S-allele in one population. The correlations evaluated by a GLM are*
943 *represented by lines, with confidence intervals represented in grey. The dominance was considered as*
944 *a continuous variable. A: A. halleri. Black dots correspond to the Nivelle population, grey dots to the*
945 *Mortagne population. B: A. lyrata. Red dots correspond to the IND population, black dots to the PIN*
946 *population, blue dots to the TSS population.*

947 ***Figure 5: Stochastic simulations confirm the contrasted architecture of the load of deleterious***
948 ***mutations linked to dominant vs. recessive S-alleles.*** *Number of fixed (A), segregating (B) and total*
949 *(C) deleterious mutations linked to S-alleles at four different levels of dominance (I<II<III<IV). The*
950 *means (bold lines) were estimated per S-allele dominance classes over 100 replicate simulations after*
951 *discarding an initial burn-in of 100,000 generations. h=0. s=0.01.*

952

953

954 ***Tables List***

955 ***Table 1: Proportion of S-locus homozygous offspring having reached the reproductive stage for three***
956 ***different S-alleles.*** *The test is performed relative to the expected proportion of homozygous genotypes*
957 *in the offspring (25% when both parents are heterozygous; 50% when one of the parents is*
958 *homozygous and the other heterozygous).*

***S*-allele**	**Level of dominance**	**Number of seedlings having reached the reproductive stage**	**Observed proportion of homozygotes**	**Ratio of the observed to expected proportion of homozygous genotypes (*p*-value[a])**	**Number of heterozygotes with the *S*-allele (*p*-values[a])**
Ah01	I	35	0.29	1.14 (0.76)	19 (0.40; 0.90)
Ah03	II	27	**0.074**	**0.3 (0.02)**	17 (1; 0.69)
Ah04	III	96	0.479	0.96 (0.39)	50

959 *[a] p-values were obtained after 10,000 random permutations, respectively. Values departing from*
960 *Mendelian expectations are figured in bold. For Ah04, the maternal parent was Ah04/Ah04, so all*
961 *heterozygous offspring carried the S-allele.*

962

963

964

965

966

967

968

969

970

971

972

973

974

975

976

977

978

Supplementary data

Figures legend

Figure S1: Analysis of Major Components obtained for haplotypes of A. halleri of the Nivelle (black dots) and Mortagne (grey dots) populations) based on SNPs in the first 5kb, between 5 and 25kb, and between 25kb and 50kb away from the S-locus. *The S-allele to which the SNPs are linked are represented by different symbols. The right panels show the analysis on control regions, each time matching the number of SNPs with that of the corresponding linked regions (left panels).*

Figure S2: Analysis of major components (AMC) obtained for haplotypes of A. lyrata (of the PIN: grey dots, IND: red dots and TSS: blue dots) populations based on the SNPs in the first 5kb, between 5 and 25kb, and between 25kb and 50kb away from the S-locus. *The S-allele to which the SNPs are linked are represented by different symbols. The right panels show the analysis on control regions, each time matching the number of SNPs with that of the corresponding linked regions (left panels).*

Figure S3: Phylogenetic tree obtained by Maximum Likelihood for haplotypes of A. halleri (populations Nivelle and Mortagne) across the first 25kb flanking the S-locus. *The Tamura-Nei model was used and the percentage of trees in which the associated haplotypes clustered together is shown next to the branches. The tree is drawn to scale, with branch lengths measured in the number of substitutions per site. The black braces indicate haplotypes clustering by populations. The overall pattern shows a structure by S-alleles, with exceptions highlighted in yellow.*

Figure S4: Phylogenetic tree obtained by maximum likelihood for haplotypes of A. halleri (populations Nivelle and Mortagne) based on the nucleotide positions between 25kb and 50kb away from the S-locus. *The Tamura-Nei model was used and the percentage of trees in which the associated haplotypes clustered together is shown next to the branches. The tree is drawn to scale, with branch lengths measured in the number of substitutions per site. The black braces indicate haplotypes clustering by populations. The overall pattern shows a structure by S-alleles, with exceptions highlighted in yellow.*

Figure S5: Phylogenetic tree obtained by maximum likelihood for haplotypes of A. lyrata (populations PIN, IND, TSS) across the first 5kb flanking the S-locus. *The Tamura-Nei model was used and the percentage of trees in which the associated haplotypes clustered together is shown next to the branches. The tree is drawn to scale, with branch lengths measured in the number of substitutions per site. The black braces indicate haplotypes clustering by populations. The overall pattern shows a structure by S-alleles, with exceptions highlighted in yellow.*

Figure S6: Phylogenetic tree obtained by maximum likelihood for haplotypes of A. lyrata (populations PIN, IND, TSS) based on the nucleotide positions between 5kb and 10kb away from the S-locus. *The Tamura-Nei model was used and the percentage of trees in which the associated haplotypes clustered together is shown next to the branches. The tree is drawn to scale, with branch lengths measured in the number of substitutions per site. The black braces indicate haplotypes clustering by populations. The overall pattern shows a structure by S-alleles, with exceptions highlighted in yellow.*

1017 ***Figure S7: The genetic structure of SNPs in the S-locus flanking regions in A. halleri and A. lyrata.***
1018 *Left: Mean F_{ST} (lines) and F_{ST} by pair (point) analysed among S-alleles (grey) or among populations*
1019 *(black) in 5 kb windows in the S-locus flanking regions. Right: Distribution (count) of F_{ST} in the control*
1020 *regions analysed among S-alleles (grey bars) or among populations (black bars). The 95% percentiles*
1021 *of the distributions are represented by dotted lines and the medians by solid lines.*

1022 ***Figure S8: Patterns of genetic associations between S-alleles and SNPs across the genome.*** *Each dot*
1023 *corresponds to a SNP showing statistically significant association (top 0.1%) with a given S-allele. The*
1024 *left panel confirms that SNPs physically linked to the S-locus (in red) are considerably more likely to*
1025 *show statistical associations with S-alleles. The chromosomes were signified by alternance of black and*
1026 *grey. The middle panel shows a zoom on the 50kb regions flanking the S-locus and shows that the*
1027 *statistical association extends over long distances, at least for some S-alleles. Each region of 25 kb was*
1028 *delimited by vertical lines. The right panel shows that the observed number of associated SNPs in the*
1029 *linked regions far exceeds that in regions of identical size from control regions. The histogram shows*
1030 *the distribution across control regions of the mean number of significantly associated SNPs per S-allele.*
1031 *The vertical lines correspond to the mean number of significantly associated SNPs in the first 25kb*
1032 *(solid lines) and the 25-50kb interval (dashed lines) away from S-locus.).*

1033 ***Figure S9: Experimental protocol.*** *A) We randomly crossed A. lyrata individuals from the PIN, TSS and*
1034 *IND populations in North America (left) and A. halleri from the Nivelle (middle) and Mortagne (right)*
1035 *populations. Individuals were sequenced by a capture protocol. Numbers between parentheses*
1036 *represent the number of individuals per dataset. B) One offspring from each cross was sequenced along*
1037 *with its two parents for trio haplotyping. Offspring from the Nivelle population (black circle) were*
1038 *conserved for the study of the impact of homozygosity at the S-locus on fitness (G1 population).*
1039 *C)Individuals sequenced in A and B were used to reconstruct haplotypes linked to each copy of S-allele,*
1040 *assuming no recombination between the S-locus and its flanking regions between parents and*
1041 *offspring. D) We used the dominance hierarchy between S-alleles expressed in pollen to cross G1*
1042 *individuals from the Nivelle population and obtained six G2 families constituted of heterozygous and*
1043 *homozygous individuals for the alleles Ah01 , Ah03 and Ah04 . E) Description of the traits measured,*
1044 *and the methods used to estimate the impact of homozygosity at the S-locus in homozygotes. Traits 1-*
1045 *8 are related to biomass and traits 10-14 are related to reproductive success.*

1046
1047

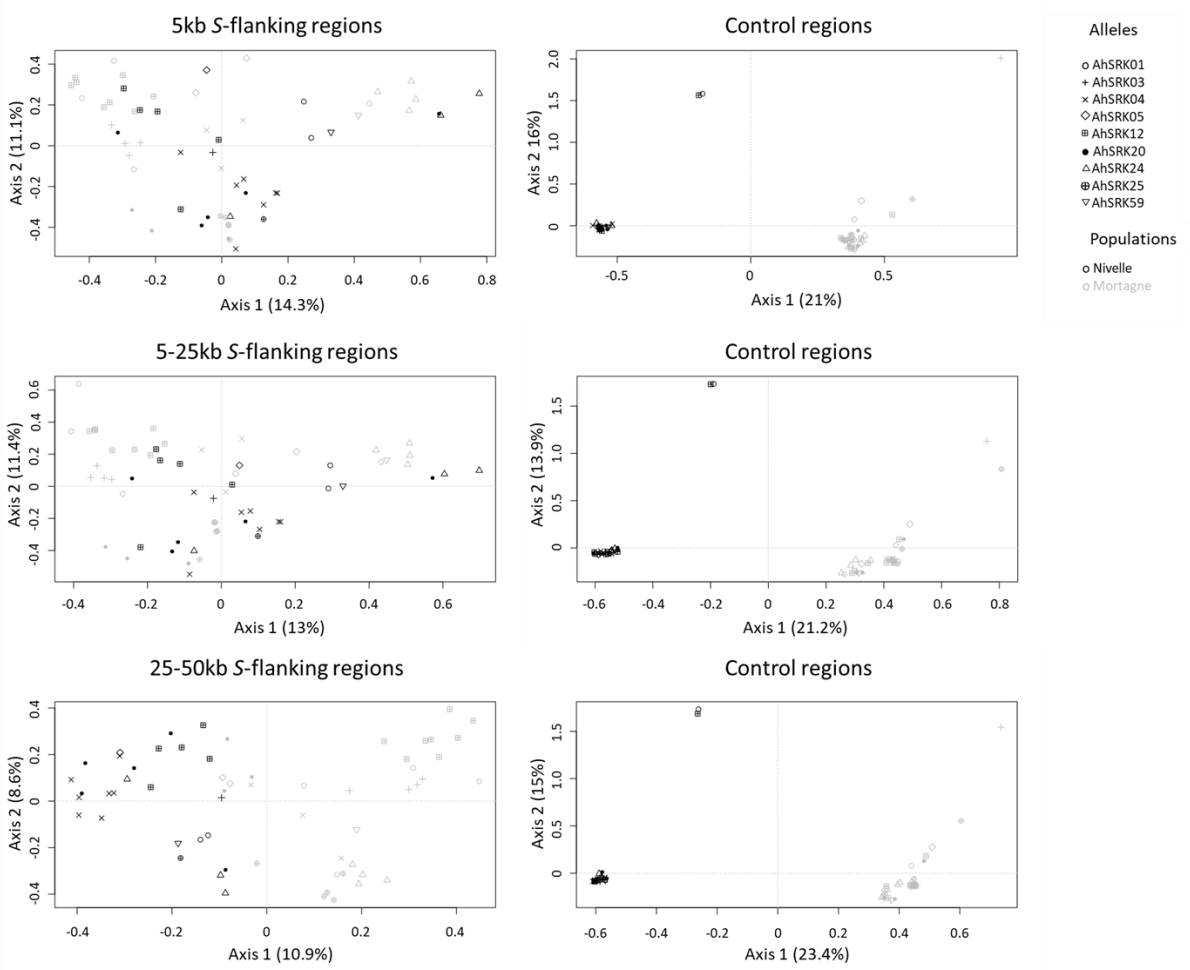

Figure S1: Analysis of Major Components obtained for haplotypes of A. halleri of the Nivelle (black dots) and Mortagne (grey dots) populations) based on SNPs in the first 5kb, between 5 and 25kb, and between 25kb and 50kb away from the S-locus.

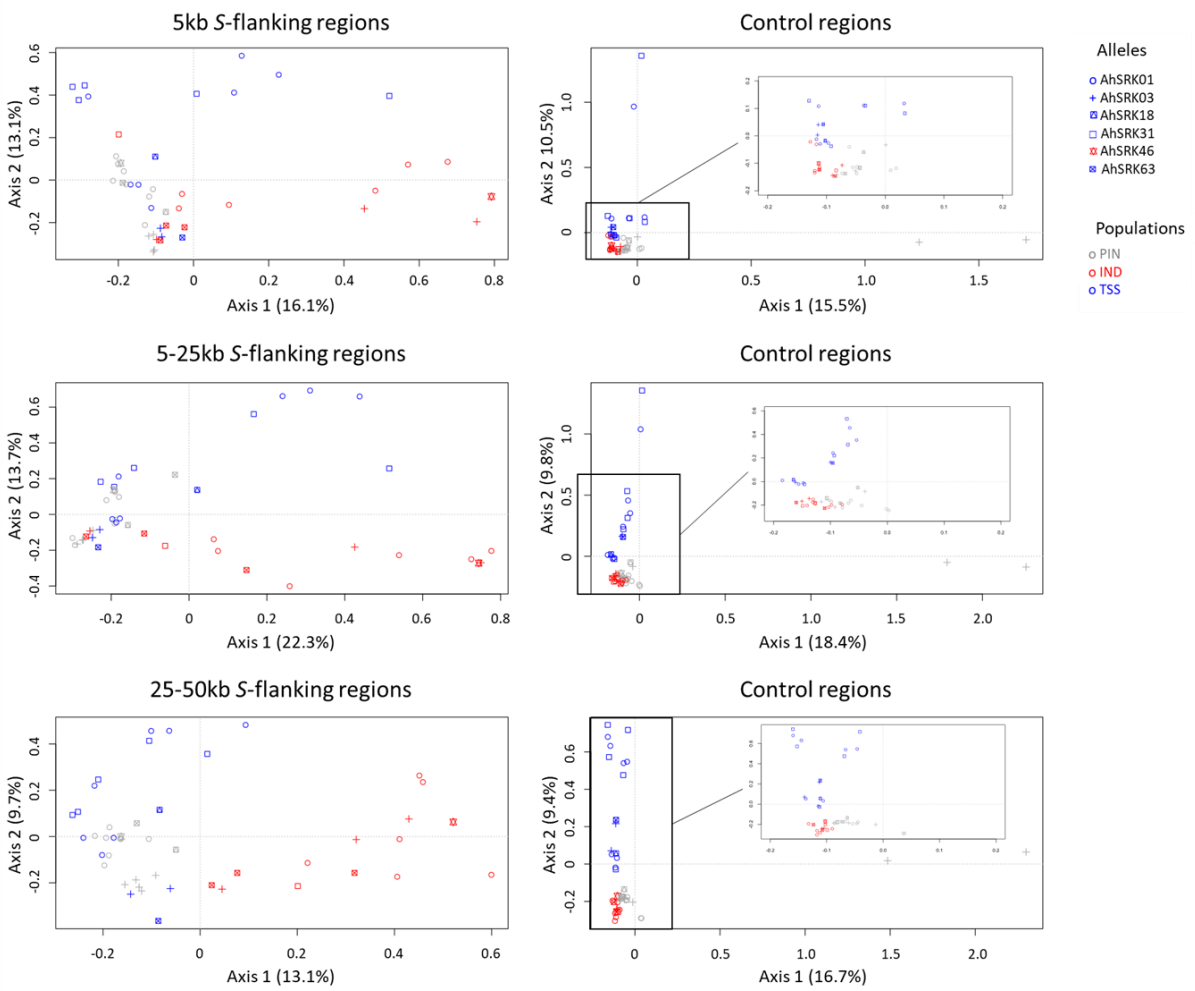

Figure S2: Analysis of major components (AMC) obtained for haplotypes of A. lyrata (of the PIN: grey dots, IND: red dots and TSS: blue dots) populations based on the SNPs in the first 5kb, between 5 and 25kb, and between 25kb and 50kb away from the S-locus.

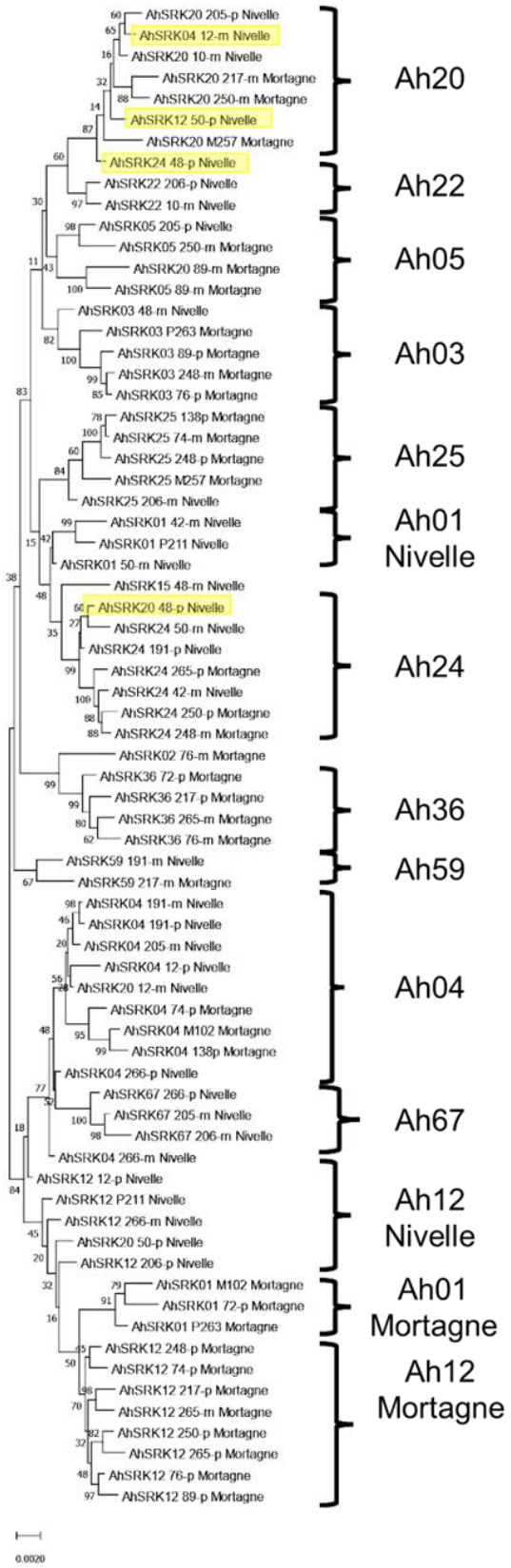

Figure S3: Phylogenetic tree obtained by Maximum Likelihood for haplotypes of A. halleri (populations Nivelle and Mortagne) across the first 25kb flanking the S-locus.

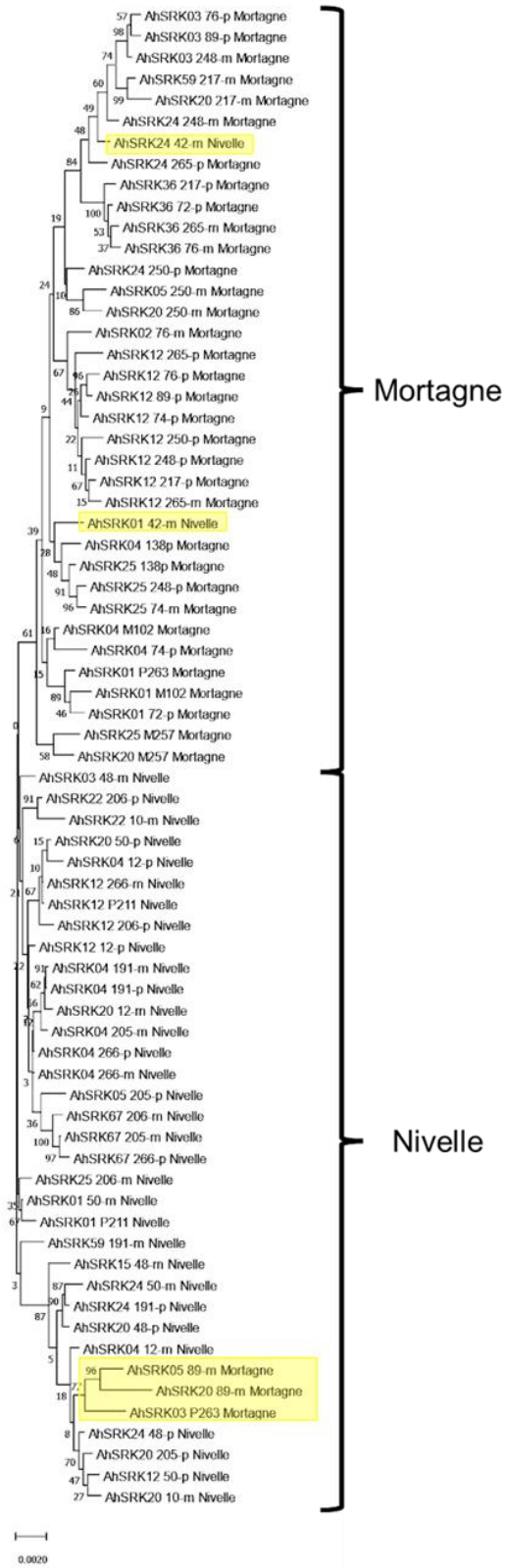

Figure S4: Phylogenetic tree obtained by maximum likelihood for haplotypes of A. halleri (populations Nivelle and Mortagne) based on the nucleotide positions between 25kb and 50kb away from the S-locus.

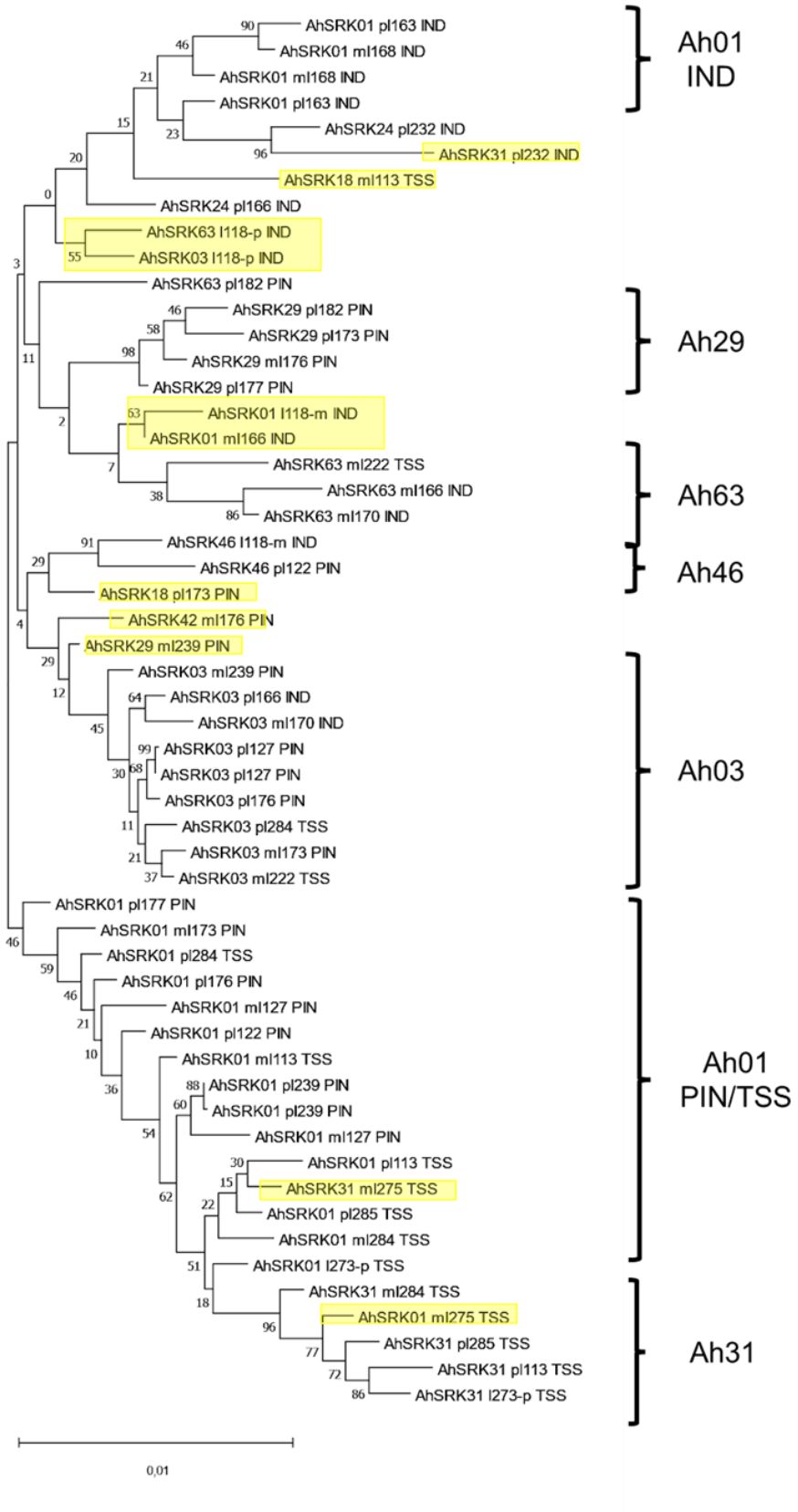

Figure S5: Phylogenetic tree obtained by maximum likelihood for haplotypes of A. lyrata (populations PIN, IND, TSS) across the first 5kb flanking the S-locus.

1066

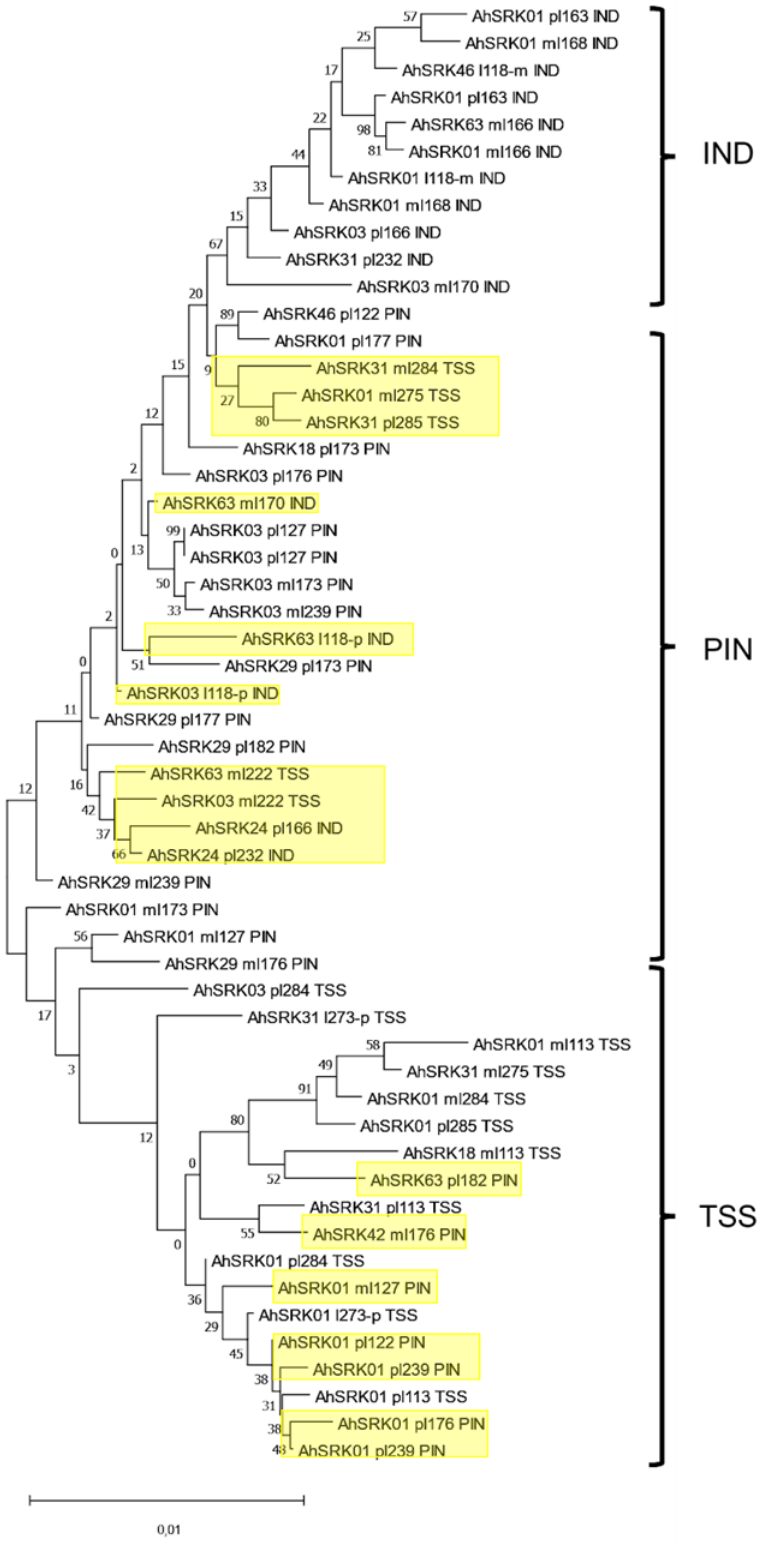

1067

1068 ***Figure S6: Phylogenetic tree obtained by maximum likelihood for haplotypes of A. lyrata***
1069 ***(populations PIN, IND, TSS) based on the nucleotide positions between 5kb and 10kb away from the***
1070 ***S-locus.***

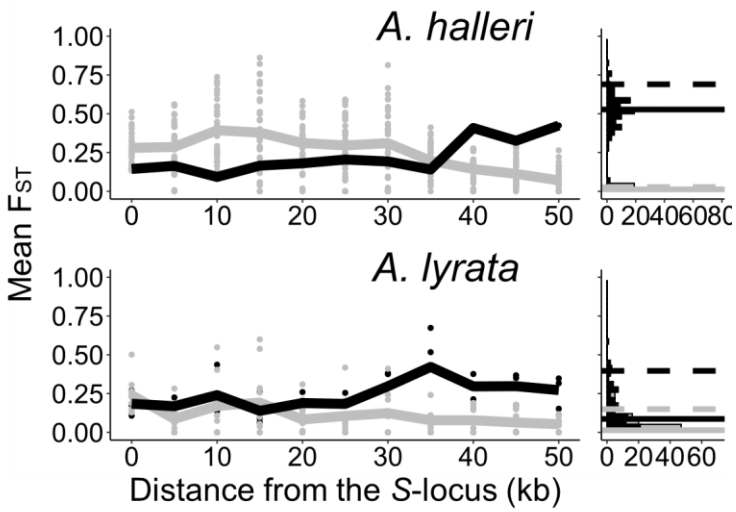

1071

1072 ***Figure S7: The genetic structure of SNPs in the S-locus flanking regions in A. halleri and A. lyrata.***

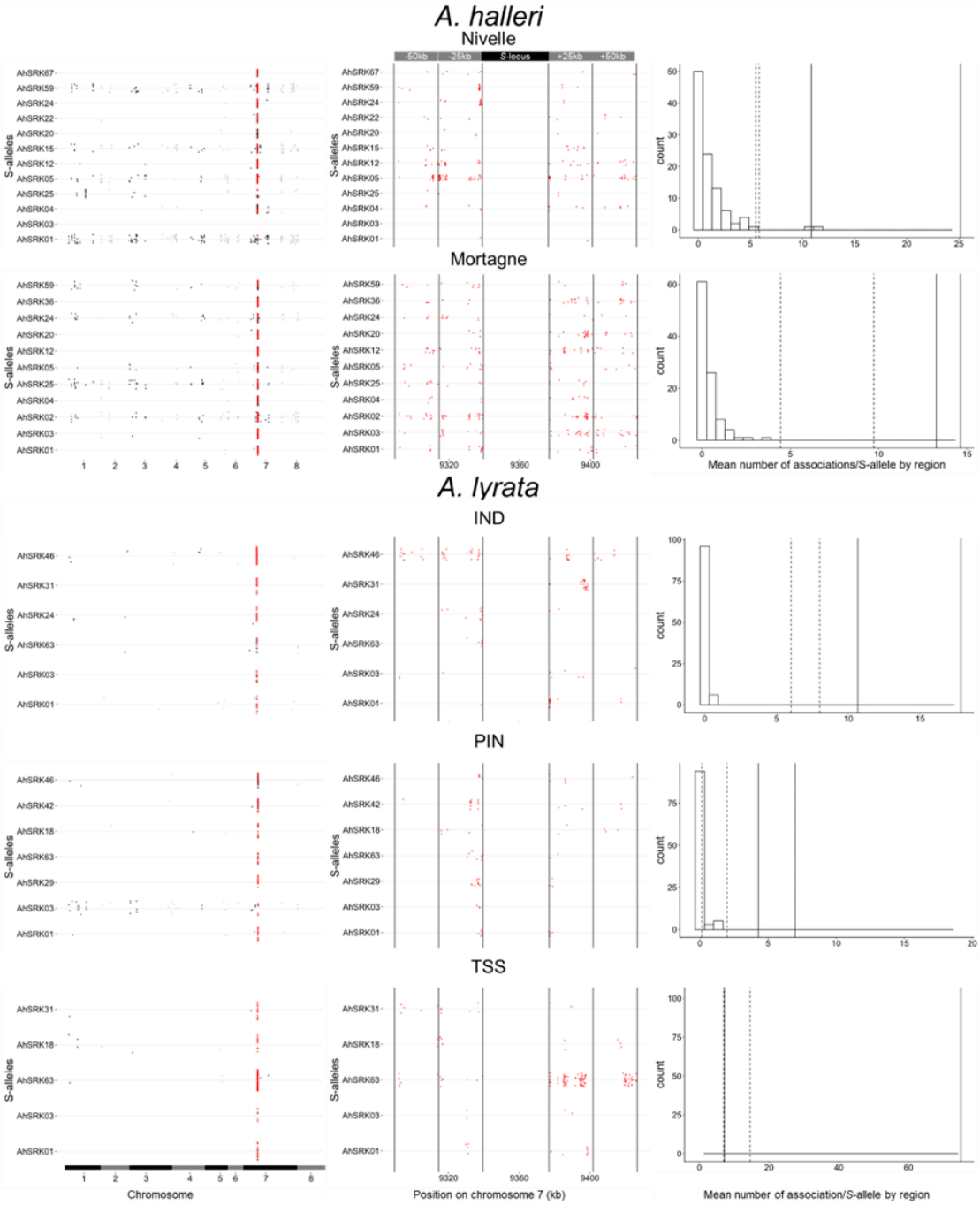

1073

1074 ***Figure S8: Patterns of genetic associations between S-alleles and SNPs across the genome.***

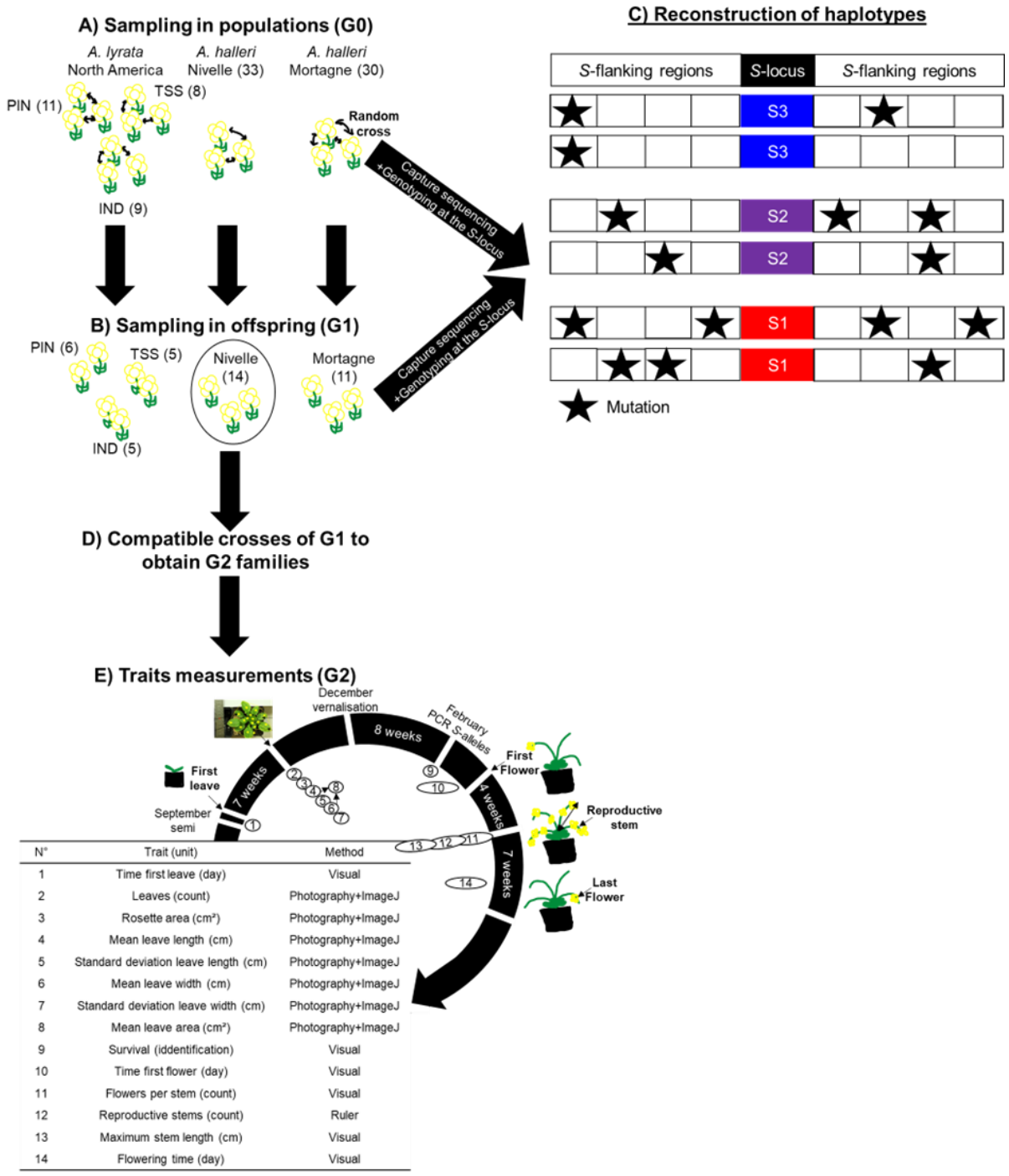

N°	Trait (unit)	Method
1	Time first leave (day)	Visual
2	Leaves (count)	Photography+ImageJ
3	Rosette area (cm²)	Photography+ImageJ
4	Mean leave length (cm)	Photography+ImageJ
5	Standard deviation leave length (cm)	Photography+ImageJ
6	Mean leave width (cm)	Photography+ImageJ
7	Standard deviation leave width (cm)	Photography+ImageJ
8	Mean leave area (cm²)	Photography+ImageJ
9	Survival (iddentification)	Visual
10	Time first flower (day)	Visual
11	Flowers per stem (count)	Visual
12	Reproductive stems (count)	Ruler
13	Maximum stem length (cm)	Visual
14	Flowering time (day)	Visual

1075

1076 ***Figure S9: Experimental protocol.***

1077

1078 ## Supplemental items

1079 ***Table S1: Crosses performed to obtain homozygotes for three S-alleles.***

1080 ***Table S2: Trait variation in S-locus homozygous individuals.***

1081 ***Table S3: Trait variation in homozygous at the S-locus for the S-alleles Ah01 and Ah04 between***
1082 ***families.***

1083 ***Table S4: Effect of dominance on variation of phenotypic traits in S-locus homozygous individuals.***

1084 ***Table S5: Number of phased haplotypes linked to S-alleles in each sample.***

1085 ***Table S6: Effect of dominance on the accumulation of genetic load in S-flanking regions.***

1086 ***Table S7: S-locus genotypes of individuals sequenced using the capture protocol.***

1087 ***Table S8: S-locus genotypes of the offspring selected for haplotype phasing and the crosses for the***
1088 ***study of phenotypic traits.***

1089 ***Table S9: Effect of phytopathogen, phytophagous attacks and oxidative stress on the phenotypic***
1090 ***traits.***

1091 ***Table S10: Difference on the phenotypic traits variation between the two families for each allele***
1092 ***tested.***

1093

1094

1095

1096

1097

1098 ***Table S1: Crosses performed to obtain homozygotes for three S-alleles.*** *For each S-allele, we*
1099 *obtained homozygous and heterozygous plants within two separate families (listed as separate*
1100 *rows).*

Genotype pollen donor [a]	*Genotype stigma recipient*	*Homozygote studied*	*Dominance level*	*Number of fruits obtained*	*Number of seeds*
Ah20/*Ah01*	*Ah12/Ah01*	*Ah01*	*1*	*5*	*48*
Ah20/*Ah01*	*Ah12/Ah01*	*Ah01*	*1*	*2*	*23*
Ah02/*Ah03*	*Ah03/Ah01*	*Ah03*	*2*	*6*	*69*
Ah24/*Ah03*	*Ah03/Ah01*	*Ah03*	*2*	*3*	*27*
Ah20/*Ah04*	*Ah04/Ah04*	*Ah04*	*3*	*21*	*167*
Ah20/*Ah04*	*Ah04/Ah04*	*Ah04*	*3*	*8*	*65*

1101 *[a] The S-alleles in bold represent the dominant S-allele expressed on pollen of each donor genotype.*
1102 *Each line corresponds to one pair of individuals used as parents.*

1103

1104

1105

1106 ***Table S2: Trait variation in S-locus homozygous individuals.***

Trait (unit)	*Mean heterozygotes (SD)*	*Mean homozygotes (SD)*	*P value* [a]
Time first leaf (day)	*15.7 (1.04)*	*14.79 (1.19)*	*0.14*
Number of leaves	*13.22 (0.65)*	*13.46 (0.96)*	*0.35*
Rosette area (cm²)	*34.99 (5.11)*	*35.5 (7.65)*	*0.46*
Mean leaf length (cm)	*1.86 (0.15)*	*1.86 (0.21)*	*0.49*
St dev leaf length (cm)	*0.28 (0.02)*	*0.29 (0.04)*	*0.31*
Mean leaf width (cm)	*1.49 (0.11)*	*1.46 (0.14)*	*0.36*
St dev leaf width (cm)	*0.27 (0.02)*	*0.25 (0.03)*	*0.24*
Mean leaf area (cm²)	*3.16 (0.43)*	*3.11 (0.6)*	*0.45*
Time first flower (day)	*36.28 (1.14)*	*34.98 (1.25)*	*0.07*
Number of flowering stems	*12.9 (0.91)*	*13.3 (1.32)*	*0.31*
Maximum flowering stem length (cm)	***56.19 (2.26)***	***64.55 (3.17)***	***<1e^{-04}***
Number of flowers by flowering stem	*58.87 (5.96)*	*66.56 (10.71)*	*0.09*
Flowering duration (day)	*44.15 (1.7)*	*43.81 (1.88)*	*0.39*

1107 *[a] The P value represents the proportions of the distribution with the expected difference of mean*
1108 *between heterozygotes and homozygotes at the S-locus after 10,000 random resamples equal to or*
1109 *less than the value observed. Significant values are represented in bold.*

1110
1111
1112
1113
1114

1115 ***Table S3: Trait variation in homozygous at the S-locus for the S-alleles Ah01 and Ah04 between***
1116 ***families.***

Allele	Trait (unit)	Mean first familly (SD)	Mean second familly (SD)	p value
Ah01[b]	**Time first leaf (day)**	**17.11 (2.26)**	**32 (NA)**	**<1.00^{e-04}**
	Number of leaves	14 (2.83)	9 (NA)	0.10
	Rosette area (cm²)	27.65 (18.22)	14.21 (NA)	0.50
	Mean leaf length (cm)	1.64 (0.68)	1.52 (NA)	0.49
	St dev leaf length (cm)	0.28 (0.11)	0.17 (NA)	0.30
	Mean leaf width (cm)	1.38 (0.43)	1.38 (NA)	0.49
	St dev leaf width (cm)	0.24 (0.07)	0.16 (NA)	0.30
	Mean leaf area (cm²)	2.52 (1.59)	2.1 (NA)	0.50
	Time first flower (day)	35.86 (3.13)	36 (NA)	0.25
	Number of flowering stems	12.29 (3.9)	7 (NA)	0.25
	Maximum flowering stem length (cm)	**43.43 (6.91)**	**62.4 (NA)**	**<1.00^{e-04}**
	Number of flowers by flowering stem	31.73 (24.16)	52.25 (NA)	0.12
	Flowering duration (day)	**44.71 (6.73)**	**52 (NA)**	**<1.00^{e-04}**
Ah04	Time first leaf (day)	13.15 (2.68)	14.88 (4.36)	0.11
	Number of leaves	13.43 (2.99)	14.04 (3.9)	0.24
	Rosette area (cm²)	36.63 (27.74)	45.86 (33.48)	0.08
	Mean leaf length (cm)	1.93 (0.81)	2.13 (0.89)	0.14
	St dev leaf length (cm)	0.29 (0.15)	0.3 (0.12)	0.33
	Mean leaf width (cm)	1.54 (0.57)	1.44 (0.51)	0.20
	St dev leaf width (cm)	**0.28 (0.13)**	**0.22 (0.09)**	**0.02**
	Mean leaf area (cm²)	3.4 (2.45)	3.46 (2.27)	0.45
	Time first flower (day)	35.57 (4.73)	33.2 (3.66)	0.06
	Number of flowering stems	**13.21 (4.25)**	**16.4 (5.25)**	**0.02**
	Maximum flowering stem length (cm)	64.98 (9.65)	62.41 (9.34)	0.13
	Number of flowers by flowering stem	**72.38 (33.07)**	**45.25 (15.45)**	**1.00^{e-04}**
	Flowering duration (day)	43.68 (6.96)	41.56 (7.38)	0.23

1117 *[a] The P value represents the proportions of the distribution with the expected difference of mean*
1118 *between each family after 10,000 random resamples equal to or less than the observed value.*
1119 *Significant values are represented in bold. The Ah03 S-allele is excluded because only two*
1120 *homozygotes survived. [b] the standard deviation for the second family was not estimated because*
1121 *only one homozygote survived.*

1122 ***Table S4: Effect of dominance on variation of phenotypic traits in S-locus homozygous individuals.***

Trait (unit)	***Random effect implemented in GLM model***	***Distribution of trait tested***	***Linear effect***	***p value***
Time first leaf (days)	***Family***	***Poisson***	***-0.15***	***5.5^{e-04}***
Leaves (counts)	*Oxydative stress*	*Poisson*	*0.006*	*0.91*
Rosette area (cm²)	*Oxydative stress + family*	*Gaussian*	*8.25*	*0.19*
Mean leave length (cm)	*Oxydative stress + family*	*Gaussian*	*0.17*	*0.28*
St dev leave length (cm)	*None*	*Gaussian*	*0.02*	*0.54*
Mean leave width (cm)	*Oxydative stress + phytophagous attack*	*Gaussian*	*0.05*	*0.83*
St dev leave width (cm²)	*Oxydative stress + phytophagous attack*	*Gaussian*	*0.01*	*0.91*
Mean leave area (cm²)	*Oxydative stress*	*Gaussian*	*0.39*	*0.36*
Time first flower (days)	*Phytopathogen + phytophagous attack + family*	*Poisson*	*-0.0002*	*1*
Flowering stems (counts)	*Family*	*Poisson*	*0.15*	*0.08*
Maximum flowering stem length (cm)	*Phytopathogen + family*	*Gaussian*	*7.6*	*0.06*
Flowers by stem (counts)	*Family*	*Poisson*	*0.15*	*0.44*
Flowering duration (days)	*Phytopathogen + family*	*Poisson*	*-0.05*	*0.1*

1123 *Dominance at the S-locus was implemented as a fixed effect. The dominance was considered a*
1124 *continuous variable.*

1125

1126

1127

1128 ***Table S5: Number of phased haplotypes linked to S-alleles in each sample.***

Species	Population	Number of phased haplotypes	Number of *S*-alleles	Number of *S*-alleles with more than one copy	Mean number of gene copies per *S*-allele [a]
A. halleri	Nivelle	34	12	7	4.1
	Mortagne	38	11	9	4
A. lyrata	TSS	16	5	3	4.7
	IND	16	6	4	3.5
	PIN	22	7	3	6

1129 [a] *based on S-alleles with more than one copy.*

1130

1131 ***Table S6: Effect of dominance on the accumulation of genetic load in S-flanking regions.***

Type of mutations	Species	Number of variable sites	Genetic load estimated	Linear effect	p value
0fold	*A. halleri*	369	**Number of fixed mutations by S-allele**	**0.08**	**2.57^{e-04}**
			Number of segregating mutations by S-allele	**-0.49**	**2.21^{e-03}**
			Mean total number of mutation by S-allele (S_{0f})	0.01	0.54
	A. lyrata	243	**Number of fixed mutations by S-allele**	**0.08**	**4.50^{e-03}**
			Number of segregating mutations by S-allele	-0.44	0.09
			Mean total number of mutation by S-allele (S_{0f})	-0.07	0.07
4fold	*A. halleri*	292	**Number of fixed mutations by S-allele**	**0.23**	**8.95^{e-04}**
			Number of segregating mutations by S-allele	**-0.48**	**2.02^{e-10}**
			Mean total number of mutation by S-allele (S_{4f})	1.53^{e-03}	0.95
	A. lyrata	189	**Number of fixed mutations by S-allele**	**0.23**	**8.95^{e-04}**
			Number of segregating mutations by S-allele	**-0.46**	**0.04**
			Mean total number of mutation by S-allele (S_{4f})	-0.04	0.32
S_{0f}/S_{4f}	*A. halleri*		Ratio	0.02	0.42
	A. lyrata		Ratio	-0.11	0.11
Non-synonymous	*A. halleri*	376	**Number of fixed mutations by S-allele**	**0.10**	**6.36^{e-05}**
			Number of segregating mutations by S-allele	**-0.09**	**2.98^{e-03}**
			Mean total number of mutation by S-allele (S_{NS})	0.03	0.07
	A. lyrata	250	**Number of fixed mutations by S-allele**	**0.24**	**1.74^{e-08}**
			Number of segregating mutations by S-allele	-0.01	0.89
			Mean total number of mutation by S-allele (S_{NS})	**-0.11**	**2.06^{e-16}**
Synonymous	*A. halleri*	546	**Number of fixed mutations by S-allele**	**0.10**	**4.36^{e-07}**
			Number of segregating mutations by S-allele	**-0.12**	**3.74^{e-07}**
			Mean total number of mutation by S-allele (S_S)	**0.03**	**0.02**
	A. lyrata	369	**Number of fixed mutations by S-allele**	**0.27**	**2.3^{e-11}**
			Number of segregating mutations by S-allele	**-0.17**	**3.42^{e-03}**
			Mean total number of mutation by S-allele (S_S)	**-0.11**	**3.06^{e-25}**
S_{NS}/S_S	*A. halleri*		Ratio	-5.82^{e-03}	0.81
	A. lyrata		Ratio	0.02	0.60
Deleterious SIFT4G	*A. halleri*	58	Number of fixed mutations by S-allele	0.28	0.06
			Number of segregating mutations by S-allele	0.01	0.47
			Mean total number of mutation by S-allele (S_D)	0.02	0.69
	A. lyrata	33	**Number of fixed mutations by S-allele**	**0.66**	**3.36^{e-06}**
			Number of segregating mutations by S-allele	**-0.05**	**0.01**

			Mean total number of mutation by S-allele (S_D)	-0.10	5.48^{e-02}
Lowly deleterious SNPeff	*A. halleri*	548	**Number of fixed mutations by S-allele**	**0.09**	**1.34^{e-06}**
			Number of segregating mutations by S-allele	**-0.12**	**1.46^{e-06}**
			Mean total number of mutation by S-allele (S_{LD})	**0.03**	**0.02**
	A. lyrata	373	**Number of fixed mutations by S-allele**	**0.17**	**1.34^{e-13}**
			Number of segregating mutations by S-allele	**-0.17**	**0.47^{E-03}**
			Mean total number of mutation by S-allele (S_{LD})	**-0.11**	**3.51^{e-25}**
Moderately deleterious SNPeff	*A. halleri*	376	**Number of fixed mutations by S-allele**	**0.11**	**1.31^{e-05}**
			Number of segregating mutations by S-allele	**-0.10**	**6.39^{e-06}**
			Mean total number of mutation by S-allele (S_{MD})	0.03	0.07
	A. lyrata	247	**Number of fixed mutations by S-allele**	**0.13**	**4.45^{e-06}**
			Number of segregating mutations by S-allele	-0.02	0.74
			Mean total number of mutation by S-allele (S_{MD})	**-0.11**	**2.21^{e-16}**

Dominance at the S-locus was implemented as a fixed effect. Populations were implemented as random effects. The distribution of the genetic load estimated followed a Poisson distribution, except the ratios that followed normal distributions.

1134 ***Table S7: S-locus genotypes of individuals sequenced using the capture protocol.***

Individual	*Allele 1[a]*	*Allele 2[a]*	*Population*	*Species*	*SRA*
Mor_19_13	*Ah04 (III)*	*Ah25 (III)*	*Mortagne*	*A. halleri*	*SAMN20088356*
Mor_19_14	*Ah04 (III)*	*Ah01 (I)*	*Mortagne*	*A. halleri*	*SAMN20844087*
Mor_19_19	*Ah12 (IV)*	*Ah36 (IV)*	*Mortagne*	*A. halleri*	*SAMN20088358*
Mor_19_2	*Ah03 (II)*	*Ah24 (IV)*	*Mortagne*	*A. halleri*	*SAMN20088359*
Mor_19_23	*Ah20 (IV)*	*Ah25 (III)*	*Mortagne*	*A. halleri*	*SAMN20844088*
Mor_19_24	*Ah12 (IV)*	*Ah24 (IV)*	*Mortagne*	*A. halleri*	*SAMN20088362*
Mor_19_3	*Ah03 (II)*	*Ah01 (I)*	*Mortagne*	*A. halleri*	*SAMN20844098*
Mor_19_37	*Ah59 (IV)*	*Ah20 (IV)*	*Mortagne*	*A. halleri*	*SAMN20088357*
Mor_19_38	*Ah36 (IV)*	*Ah01 (I)*	*Mortagne*	*A. halleri*	*SAMN20088371*
Mor_19_4	*Ah25 (III)*	*Ah12 (IV)*	*Mortagne*	*A. halleri*	*SAMN20088360*
Mor_19_41	*Ah25 (III)*	*Ah25 (III)*	*Mortagne*	*A. halleri*	*SAMN20088372*
Mor_19_42	*Ah12 (IV)*	*Ah04 (III)*	*Mortagne*	*A. halleri*	*SAMN20088373*
Mor_19_45	*Ah36 (IV)*	*Ah02 (III)*	*Mortagne*	*A. halleri*	*SAMN20088374*
Mor_19_46	*Ah03 (II)*	*Ah12 (IV)*	*Mortagne*	*A. halleri*	*SAMN20088375*
Mor_19_51	*Ah20 (IV)*	*Ah05 (IV)*	*Mortagne*	*A. halleri*	*SAMN20088361*
Mor_19_53	*Ah36 (IV)*	*Ah12 (IV)*	*Mortagne*	*A. halleri*	*SAMN20088365*
Mor_19_54	*Ah24 (IV)*	*Ah12 (IV)*	*Mortagne*	*A. halleri*	*SAMN20088366*
Mor_19_55	*Ah20 (IV)*	*Ah05 (IV)*	*Mortagne*	*A. halleri*	*SAMN20088377*
Mor_19_56	*Ah12 (IV)*	*Ah03 (II)*	*Mortagne*	*A. halleri*	*SAMN20088378*
Niv_19_18	*Ah15 (IV)*	*Ah03 (II)*	*Nivelle*	*A. halleri*	*SAMN20088349*
Niv_19_19	*Ah20 (IV)*	*Ah24 (IV)*	*Nivelle*	*A. halleri*	*SAMN20088350*
Niv_19_22	*Ah24 (IV)*	*Ah01 (I)*	*Nivelle*	*A. halleri*	*SAMN20088351*
Niv_19_23	*Ah20 (IV)*	*Ah12 (IV)*	*Nivelle*	*A. halleri*	*SAMN20088352*
Niv_19_3	*Ah04 (III)*	*Ah59 (IV)*	*Nivelle*	*A. halleri*	*SAMN20088336*
Niv_19_31	*Ah04 (III)*	*Ah24 (IV)*	*Nivelle*	*A. halleri*	*SAMN20088337*

Niv_19_4	*Ah01 (I)*	*Ah24 (IV)*	*Nivelle*	*A. halleri*	*SAMN20088382*
Niv_19_42	*Ah22 (IV)*	*Ah12 (IV)*	*Nivelle*	*A. halleri*	*SAMN20088341*
Niv_19_45	*Ah12 (IV)*	*Ah04 (III)*	*Nivelle*	*A. halleri*	*SAMN20088344*
Niv_19_5	*Ah25 (III)*	*Ah67 (IV)*	*Nivelle*	*A. halleri*	*SAMN20088340*
Niv_19_52	*Ah20 (IV)*	*Ah22 (IV)*	*Nivelle*	*A. halleri*	*SAMN20088331*
Niv_19_53	*Ah05 (IV)*	*Ah20 (IV)*	*Nivelle*	*A. halleri*	*SAMN20088339*
Niv_19_54	*Ah01 (I)*	*Ah12 (IV)*	*Nivelle*	*A. halleri*	*SAMN20844097*
Niv_19_58	*Ah02 (III)*	*Ah59 (IV)*	*Nivelle*	*A. halleri*	*SAMN20088343*
Niv_19_59	*Ah01 (I)*	*Ah67 (IV)*	*Nivelle*	*A. halleri*	*SAMN20844096*
Niv_19_60	*Ah04 (III)*	*Ah20 (IV)*	*Nivelle*	*A. halleri*	*SAMN20088332*
Niv_19_7	*Ah04 (III)*	*Ah67 (IV)*	*Nivelle*	*A. halleri*	*SAMN20088345*
Niv_19_8	*Ah04 (III)*	*Ah12 (IV)*	*Nivelle*	*A. halleri*	*SAMN20844090*
Niv_19_9	*Ah04 (III)*	*Ah67 (IV)*	*Nivelle*	*A. halleri*	*SAMN20088338*
Pin_15_1	*Ah03 (II)*	*Ah01 (I)*	*PIN*	*A. lyrata*	*SAMN20088324*
Pin_16_1	*Ah01 (I)*	*Ah46 (IV)*	*PIN*	*A. lyrata*	*SAMN20088318*
Pin_4_24	*Ah03 (II)*	*Ah29 (III)*	*PIN*	*A. lyrata*	*SAMN20088314*
Pin_16_3	*Ah18 (IV)*	*Ah29 (III)*	*PIN*	*A. lyrata*	*SAMN20088323*
Pin_4_54	*Ah03 (II)*	*Ah03 (II)*	*PIN*	*A. lyrata*	*SAMN20088319*
Pin_5_1	*Ah01 (I)*	*Ah01 (I)*	*PIN*	*A. lyrata*	*SAMN20844102*
Pin_5_12	*Ah29 (III)*	*Ah01 (I)*	*PIN*	*A. lyrata*	*SAMN20088325*
Pin_5_2	*Ah03 (II)*	*Ah01 (I)*	*PIN*	*A. lyrata*	*SAMN20088311*
Pin_8_15	*Ah01 (I)*	*Ah01 (I)*	*PIN*	*A. lyrata*	*SAMN20088328*
Pin_8_2	*Ah29 (III)*	*Ah63 (III)*	*PIN*	*A. lyrata*	*SAMN20088326*
Pin_9_1	*Ah42 (IV)*	*Ah29 (III)*	*PIN*	*A. lyrata*	*SAMN20088312*
Tss_14_3	*Ah01 (I)*	*Ah31 (IV)*	*TSS*	*A. lyrata*	*SAMN20088315*
Tss_21_10	*Ah01 (I)*	*Ah03 (II)*	*TSS*	*A. lyrata*	*SAMN20088329*
Tss_22_24	*Ah01 (I)*	*Ah31 (IV)*	*TSS*	*A. lyrata*	*SAMN20088306*

Tss_22_7	*Ah01 (I)*	*Ah31 (IV)*	*TSS*	*A. lyrata*	*SAMN20088317*
Tss_3_10	*Ah31 (IV)*	*Ah01 (I)*	*TSS*	*A. lyrata*	*SAMN20088330*
Tss_23_2	*Ah03 (II)*	*Ah63 (III)*	*TSS*	*A. lyrata*	*SAMN20088313*
Tss_3_23	*Ah18 (IV)*	*Ah01 (I)*	*TSS*	*A. lyrata*	*SAMN20088307*
Tss_5_1	*Ah01 (I)*	*Ah31 (IV)*	*TSS*	*A. lyrata*	*SAMN20088316*
Ind_1_1	*Ah01 (I)*	*Ah01 (I)*	*IND*	*A. lyrata*	*SAMN20088320*
Ind_10_3	*Ah31 (IV)*	*Ah24 (IV)*	*IND*	*A. lyrata*	*SAMN20088327*
Ind_15_1	*Ah03 (II)*	*Ah24 (IV)*	*IND*	*A. lyrata*	*SAMN20088321*
Ind_15_2	*Ah63 (III)*	*Ah03 (II)*	*IND*	*A. lyrata*	*SAMN20088309*
Ind_9_3	*Ah01 (I)*	*Ah46 (IV)*	*IND*	*A. lyrata*	*SAMN20088322*
Ind_18_1	*Ah01 (I)*	*Ah01 (I)*	*IND*	*A. lyrata*	*SAMN20844103*
Ind_6_1	*Ah01 (I)*	*Ah63 (III)*	*IND*	*A. lyrata*	*SAMN20088308*
Ind_8_1	*Ah03 (II)*	*Ah63 (III)*	*IND*	*A. lyrata*	*SAMN20088305*

1135 [a] *The individuals were mainly sequenced by capture approach. The genotypes of homozygotes were*
1136 *confirmed after a whole genome sequencing. The class of dominance is specified in parenthesis.*

1137

1138

1139

1140

1141 ***Table S8: S-locus genotypes of the offspring selected for haplotype phasing and the crosses for the***
1142 ***study of phenotypic traits.***

Identity[a]	***Allele 1***	***Allele 2***	***Pollen donor[c]***	***Stigma recipient[c]***	***SRA***
d32	*Ah03*	*Ah12*	*Mor_19_2*	*Mor_19_19*	*SAMN20844104*
d33	*Ah01*	*Ah12*	*Mor_19_3*	*Mor_19_4*	*SAMN20844105*
d38[d]	*Ah04*	*Ah04*	*Mor_19_13*	*Mor_19_14*	*SAMN20844106*
d42	*Ah20*	*Ah12*	*Mor_19_23*	*Mor_19_24*	*SAMN20844107*
d72	*Ah20*	*Ah36*	*Mor_19_37*	*Mor_19_38*	*SAMN20844108*
d74	*Ah25*	*Ah12*	*Mor_19_41*	*Mor_19_42*	*SAMN20844109*
d76	*Ah03*	*Ah36*	*Mor_19_46*	*Mor_19_45*	*SAMN20844110*
d89	*Ah03*	*Ah05*	*Mor_19_56*	*Mor_19_55*	*SAMN20844111*
d217	*Ah12*	*Ah59*	*Mor_19_19*	*Mor_19_37*	*SAMN20844112*
d250	*Ah12*	*Ah20*	*Mor_19_24*	*Mor_19_51*	*SAMN20844113*
d265	*Ah36*	*Ah24*	*Mor_19_53*	*Mor_19_54*	*SAMN20844114*
d3.1	*Ah24*	*Ah25*	*Niv_19_4*	*Niv_19_5*	*SAMN20844115*
d10.1[f]	*Ah03*	*Ah24*	*Niv_19_18*	*Niv_19_19*	*SAMN20844116*
d12.1[f]	*Ah01*	*Ah20*	*Niv_19_22*	*Niv_19_23*	*SAMN20844117*
d30.1	*Ah02*	*Ah01*	*Niv_19_58*	*Niv_19_59*	*SAMN20844118*
d48.1	*Ah20*	*Ah25*	*Niv_19_52*	*Niv_19_5*	*SAMN20844119*
d50.1[e]	*Ah12*	*Ah04*	*Niv_19_8*	*Niv_19_60*	*SAMN20844120*
d51.1	*Ah12*	*Ah04*	*Niv_19_54*	*Niv_19_7*	*SAMN20844121*
d191.1[e,f]	*Ah04*	*Ah04*	*Niv_19_3*	*Niv_19_31*	*SAMN20844122*
d206.1	*Ah22*	*Ah25*	*Niv_19_42*	*Niv_19_5*	*SAMN20844123*
d205.1[f]	*Ah20*	*Ah04*	*Niv_19_53*	*Niv_19_9*	*SAMN20844124*
d208.1[f]	***Ah03***	***Ah02***	***Niv_19_58***	***Niv_19_18***	***SAMN20844125***
d17.1[f]	***Ah03***	***Ah01***	***Niv_19_33***	***Niv_19_32[b]***	***SAMN20844126***
d24.1[f]	***Ah20***	***Ah01***	***Niv_19_47[b]***	***Niv_19_46[b]***	***SAMN20844127***

d29.1[f]	***Ah12***	***Ah01***	***Niv_19_57***[b]	***Niv_19_56***[b]	***SAMN20844128***
d50.2[f]	***Ah04***	***Ah04***	***Niv_19_8***	***Niv_19_60***	***SAMN20844129***
d266.1	*Ah04*	*Ah12*	*Niv_19_7*	*Niv_19_45*	*SAMN20844130*
d122	*Ah01*	*Ah63*	*Pin_16_1*	*Pin_8_2*	*SAMN20844131*
d127	*Ah01*	*Ah03*	*Pin_5_1*	*Pin_4_54*	*SAMN20844132*
d173	*Ah03*	*Ah18*	*Pin_5_2*	*Pin_16_3*	*SAMN20844133*
d176	*Ah03*	*Ah42*	*Pin_15_1*	*Pin_9_1*	*SAMN20844134*
d177	*Ah01*	*Ah29*	*Pin_16_1*	*Pin_5_12*	*SAMN20844135*
d239	*Ah29*	*Ah01*	*Pin_4_24*	*Pin_8_15*	*SAMN20844136*
d113	*Ah18*	*Ah31*	*Tss_3_23*	*Tss_22_7*	*SAMN20844137*
d273	*Ah03*	*Ah01*	*Tss_23_2*	*Tss_22_24*	*SAMN20844138*
d275	*Ah63*	*Ah31*	*Tss_23_2*	*Tss_14_3*	*SAMN20844139*
d284	*Ah01*	*Ah31*	*Tss_21_10*	*Tss_5_1*	*SAMN20844140*
d285	*Ah01*	*Ah31*	*Tss_21_10*	*Tss_3_10*	*SAMN20844141*
d118	*Ah03*	*Ah01*	*Ind_9_3*	*Ind_8_1*	*SAMN20844142*
d163	*Ah03*	*Ah01*	*Ind_8_1*	*Ind_1_1*	*SAMN20844143*
d166	*Ah03*	*Ah01*	*Ind_6_1*	*Ind_15_1*	*SAMN20844144*
d170	*Ah01*	*Ah63*	*Ind_9_3*	*Ind_15_2*	*SAMN20844145*
d232	*Ah01*	*Ah31*	*Ind_18_1*	*Ind_10_3*	*SAMN20844146*

1143 *[a] Offspring figured in bold were not used to reconstitute haplotype of parents. [b] Parents were not*
1144 *sequenced. [c] Italics indicate parental haplotypes that were suppressed from the dataset because they*
1145 *had already been phased through another offspring . [d] The homozygous genotype of d38 was*
1146 *confirmed by genome-wide sequencing. [e] The homozygous genotypes of d191 and d50.1 were*
1147 *confirmed by the proportion of homozygous S-alleles in their offspring found by PCR after cross. [f] The*
1148 *individuals used for crosses in the phenotypic experiments.*

1149
1150
1151

1152

1153 ***Table S9: Effect of phytopathogen, phytophagous attacks and oxidative stress on the phenotypic***
1154 ***traits***

Effect tested		*Mean with attack (sd)*	*Mean without attack (sd)*	*p value* [a]
		15.37 (4.84)	*15.38 (5.24)*	*0.49*
		13.03 (2.9)	*13.46 (3.71)*	*0.23*
		31.93 (27.19)	*37.08 (27.14)*	*0.13*
		1.78 (0.78)	*1.91 (0.8)*	*0.16*
		0.29 (0.14)	*0.28 (0.13)*	*0.38*
		1.42 (0.56)	*1.51 (0.53)*	*0.17*
		0.25 (0.11)	*0.27 (0.12)*	*0.23*
		2.94 (2.33)	*3.25 (2.15)*	*0.2*
		37.43 (4.56)	***31.34 (5.55)***	***2e-03***
		12.05 (4.4)	*11.84 (4.62)*	*0.05*
	Maximum flowering stem	*56.78 (12.04)*	*52.55 (11.82)*	*0.1*
		56.56 (30.99)	*56.22 (34.55)*	*0.11*
Phytopathogen		***41.44 (8.13)***	***39.51 (7.32)***	***9e-03***
		14.48 (4.4)	*15.56 (5.2)*	*0.16*
		12.59 (3.76)	*13.44 (3.35)*	*0.13*
		32.15 (32.24)	*35.77 (26.16)*	*0.27*
		1.68 (0.83)	*1.9 (0.78)*	*0.1*
		0.29 (0.1)	*0.28 (0.14)*	*0.36*
		1.29 (0.55)	***1.51 (0.53)***	***0.03***
		0.22 (0.1)	***0.27 (0.12)***	***0.03***
		2.59 (2.3)	*3.25 (2.19)*	*0.08*
		34.78 (6.93)	***33.36 (4.92)***	***0.04***
Phytophagous	*Number of flowering stems*	*10.78 (4.76)*	*12.15 (4.55)*	*0.34*

	Maximum flowering stem	***53.53 (9.81)***	***54.24 (12.2)***	***0.05***
		47.46 (25.45)	*58.12 (34.46)*	*0.17*
		37.56 (8.1)	*40.76 (7.76)*	*0.45*
		14.92 (3.93)	*15.46 (5.28)*	*0.34*
		10.04 (3.88)	***13.93 (2.96)***	***1e-^{04}***
		11.79 (16.54)	***39.64 (26.56)***	***1e-^{04}***
		1.05 (0.49)	***2.02 (0.74)***	***1e-^{04}***
		0.25 (0.1)	*0.29 (0.14)*	*0.09*
		0.88 (0.31)	***1.59 (0.5)***	***1e-^{04}***
		0.23 (0.12)	***0.27 (0.12)***	***0.04***
		1.05 (0.98)	***3.54 (2.17)***	***1e-^{04}***
		31.77 (5.6)	*33.95 (5.25)*	*0.06*
		10.38 (4.85)	*12.21 (4.54)*	*0.44*
	Maximum flowering stem	*50.3 (13.1)*	*54.85 (11.71)*	*0.11*
		53.97 (55.98)	*56.8 (28.05)*	*0.21*
Oxidative stress	*Flowering duration (day)*	*37.35 (6.5)*	*40.78 (7.94)*	*0.08*

[a] The P value represents the proportions of the distribution with the expected difference of mean between individuals with and without attack after 10,000 random resamples equal to or less than the value observed. Significant values are represented in bold.

1159 ***Table S10: Difference on the phenotypic trait variation between the two families for each allele***
1160 ***tested.***

Allele	*Family (Male/Female)*	*Trait (unit)*	*Mean (sd)*	*p value*[a]
Ah01	*1 (d29.1/d24.1)*	***Time first leaf (day)***	***20.8 (5.43)***	***$2e^{-03}$***
		Number of leaves	*11.9 (3.75)*	*0.09*
		Rosette area (cm²)	*24.9 (25.58)*	*0.11*
		Mean leaf length (cm)	*1.53 (0.79)*	*0.08*
		St dev leaf length (cm)	*0.21 (0.09)*	*0.03*
		Mean leaf width (cm)	*1.4 (0.58)*	*0.33*
		St dev leaf width (cm)	*0.24 (0.14)*	*0.32*
		Mean leaf area (cm²)	*2.47 (1.93)*	*0.17*
		Time first flower (day)	*28.8 (5.29)*	*0.44*
		Number of flowering stems	***8 (4.07)***	***0.02***
		Maximum flowering stem length (cm)	***40.65 (6.76)***	***0.02***
		Number of flowers by flowering stem	***35.85 (10.72)***	***0.04***
		Flowering duration (day)	***40.35 (12.45)***	***$8e^{-03}$***
Ah01	*2 (d12.1/d29.1)*	***Time first leaf (day)***	***18.76 (5.57)***	***$1e^{-04}$***
		Number of leafs	*13.45 (3.22)*	*0.42*
		Rosette area (cm²)	*31.99 (22.61)*	*0.25*
		Mean leaf length (cm)	*1.74 (0.71)*	*0.19*
		St dev leaf length (cm)	*0.29 (0.1)*	*0.42*
		Mean leaf width (cm)	*1.44 (0.51)*	*0.34*
		St dev leaf width (cm)	*0.29 (0.11)*	*0.11*
		Mean leaf area (cm²)	*2.84 (1.89)*	*0.21*
		Time first flower (day)	***29.86 (5.43)***	***0.04***
		Number of flowering stems	*9.59 (3.54)*	*0.32*
		Maximum flowering stem length (cm)	***34.85 (9.35)***	***$1e^{-04}$***
		Number of flowers by flowering stem	***30.27 (25.45)***	***$1e^{-04}$***

		Flowering duration (day)	*31.62 (7.17)*	*0.06*
Ah03	*3 (d208.1/d17.1)*	*Time first leaf (day)*	*13.33 (5.27)*	*0.22*
		Number of leaves	*12.05 (4.25)*	*0.17*
		Rosette area (cm²)	*31.23 (25.7)*	*0.35*
		Mean leaf length (cm)	*1.67 (0.78)*	*0.32*
		St dev leaf length (cm)	*0.28 (0.15)*	*0.42*
		Mean leaf width (cm)	*1.39 (0.62)*	*0.5*
		St dev leaf width (cm)	*0.24 (0.13)*	*0.42*
		Mean leaf area (cm²)	*2.87 (2.24)*	*0.45*
		Time first flower (day)	***34.81 (7.87)***	***0.02***
		Number of flowering stems	***7.67 (3)***	***3e^{-04}***
		Maximum flowering stem length (cm)	***44.4 (13.87)***	***0.03***
		Number of flowers by flowering stem	*61.55 (46.06)*	*0.06*
		Flowering duration (day)	***39 (6.6)***	***5e^{-03}***
Ah03	*4 (d10.1/d17.1)*	Time first leaf (day)	18 (6.2)	0.12
		Number of leaves	12.33 (4.46)	0.22
		Rosette area (cm²)	**17.71 (11.23)**	**0.04**
		Mean leaf length (cm)	1.52 (0.53)	0.14
		St dev leaf length (cm)	0.23 (0.07)	0.14
		Mean leaf width (cm)	1.23 (0.35)	0.13
		St dev leaf width (cm)	0.23 (0.08)	0.23
		Mean leaf area (cm²)	2.01 (1.34)	0.1
		Time first flower (day)	33.33 (4.23)	0.09
		Number of flowering stems	11.67 (4.23)	0.22

		Maximum flowering stem length (cm)	57.25 (3.69)	0.34
		Number of flowers by flowering stem	75.05 (29.69)	0.12
		Flowering duration (day)	45.5 (8.67)	0.33
Ah04	*5 (d205.1/d191.1)*	***Time first leaf (day)***	***13.42 (3.28)***	***1e^{-04}***
		Number of leaves	*13.45 (2.97)*	*0.32*
		Rosette area (cm²)	*36.29 (27.39)*	*0.31*
		Mean leaf length (cm)	*1.92 (0.8)*	*0.22*
		St dev leaf length (cm)	*0.29 (0.15)*	*0.34*
		Mean leaf width (cm)	*1.54 (0.56)*	*0.11*
		St dev leaf width (cm)	*0.27 (0.13)*	*0.15*
		Mean leaf area (cm²)	*3.36 (2.41)*	*0.14*
		Time first flower (day)	*35.1 (4.66)*	*0.33*
		Number of flowering stems	*12.87 (4.16)*	*0.32*
		Maximum flowering stem length (cm)	***62.96 (9.48)***	***1e^{-04}***
		Number of flowers by flowering stem	***70.13 (32.5)***	***1e^{-04}***
		Flowering duration (day)	*42.44 (7.05)*	*0.3*
Ah04	*6 (d205.1/d50.2)*	*Time first leaf (day)*	*14.31 (4.36)*	*0.30*
		Number of leaves	*13.5 (3.9)*	*0.13*
		Rosette area (cm²)	***44.1 (33.48)***	***0.02***
		Mean leaf length (cm)	***2.04 (0.89)***	***0.04***
		St dev leaf length (cm)	*0.29 (0.12)*	*0.21*
		Mean leaf width (cm)	*1.38 (0.51)*	*0.36*
		St dev leaf width (cm)	***0.21 (0.09)***	***0.03***
		Mean leaf area (cm²)	*3.33 (2.27)*	*0.21*
		Time first flower (day)	***31.92 (3.66)***	***2e^{-03}***
		Number of flowering stems	***15.77 (5.25)***	***1e^{-04}***
		Maximum flowering stem length (cm)	*60.01 (9.34)*	*0.07*

Number of flowers by flowering stem	***43.51 (15.45)***	***$5e^{-04}$***
Flowering duration (day)	***39.96 (7.38)***	***0.04***

[a] The P value represents the proportions of the distribution with the expected difference of mean between each family and the other individuals after 10,000 random resamples equal to or less than the value observed. Significant values are represented in bold.